

XN-NF-80-19 (NP)

VOLUME 2B

**EXXON NUCLEAR METHODOLOGY FOR
BOILING WATER REACTORS -**

VOLUME 2B

**FLEX: A COMPUTER CODE FOR JET PUMP BWR
REFILL AND REFLOOD ANALYSIS**

JULY 1980

RICHLAND, WA 99352

EXXON NUCLEAR COMPANY, Inc.

8009260504

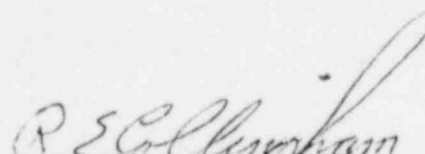
07/31/80

FLEX:

A COMPUTER CODE FOR JET PUMP BWR REFILL AND REFLOOD ANALYSIS

By: T. A. Bjornard
L. R. Zimmerman

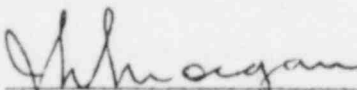
APPROVED:



R. E. Collingham, Manager
Systems Model Development

5/23/80
Date

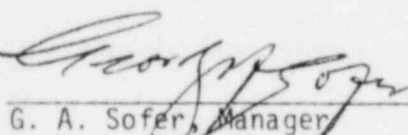
APPROVED:



J. N. Morgan, Manager
Licensing and Safety Engineering

5-27-80
Date

APPROVED:



G. A. Sofer, Manager
Nuclear Fuels Engineering

5-29-80
Date

May 1980

EXXON NUCLEAR COMPANY, Inc.

NUCLEAR REGULATORY COMMISSION DISCLAIMER

IMPORTANT NOTICE REGARDING CONTENTS AND USE OF THIS DOCUMENT

PLEASE READ CAREFULLY

This technical report was derived through research and development programs sponsored by Exxon Nuclear Company, Inc. It is being submitted by Exxon Nuclear to the USNRC as part of a technical contribution to facilitate safety analyses by licensees of the USNRC which utilize Exxon Nuclear-fabricated reload fuel or other technical services provided by Exxon Nuclear for light water power reactors and it is true and correct to the best of Exxon Nuclear's knowledge, information, and belief. The information contained herein may be used by the USNRC in its review of this report, and by licensees or applicants before the USNRC which are customers of Exxon Nuclear in their demonstration of compliance with the USNRC's regulations.

Without derogating from the foregoing, neither Exxon Nuclear nor any person acting on its behalf:

- A. Makes any warranty, express or implied, with respect to the accuracy, completeness, or usefulness of the information contained in this document, or that the use of any information, apparatus, method, or process disclosed in this document will not infringe privately owned rights; or
- B. Assumes any liabilities with respect to the use of, or for damages resulting from the use of, any information, apparatus, method, or process disclosed in this document.

KEY TO REPORT OF
EXXON NUCLEAR METHODOLOGY FOR BOILING WATER REACTORS
XN-NF-80-19(P)

- Volume 1 Exxon Nuclear Methodology for Boiling Water Reactors -
 Neutronics Methods for Design and Analysis
- Volume 2 Exxon Nuclear Methodology for Boiling Water Reactors -
 EXEM: ECCS Evaluation Model, Summary Description
- Volume 2A RELAX: A RELAP4 Based Computer Code for Calculating
 Blowdown Phenomena
- Volume 2B FLEX: A Computer Code for Jet Pump BWR Refill and
 Reflood Analysis
- Volume 3 Exxon Nuclear Methodology for Boiling Water Reactors -
 Thermal Hydraulics

ACKNOWLEDGMENTS

The significant contributions of Dr. R. T. Jensen, Dr. D. C. Mecham and Dr. E. C. Lemmon of Intermountain Technologies, Inc. and Mr. C. A. McMonagle of D. S. Rowe and Associates are gratefully acknowledged.

TABLE OF CONTENTS

	<u>Page No.</u>
1.0 INTRODUCTION AND SUMMARY	1
1.1 CORE MODEL	2
1.2 BYPASS MODEL	3
1.3 SYSTEM MODEL	3
1.4 APPLICATION	4
2.0 FLEX SOLUTION SCHEME	7
2.1 GOVERNING EQUATIONS	7
2.2 NUMERICAL SOLUTION	11
2.3 TREATMENT OF CORE AND BYPASS REGIONS IN SYSTEM NUMERICAL SOLUTION	12
3.0 FLEX CORE MODEL	15
3.1 THE PHYSICAL PHENOMENA	15
3.2 CONSERVATION EQUATIONS	16
3.2.1 CONSERVATION OF MASS	18
3.2.2 CONSERVATION OF ENERGY	20
3.2.3 CONSERVATION OF MOMENTUM	21
3.2.4 HEAT TRANSFER FROM SOLID COMPONENTS.	24
3.3 HEAT TRANSPORT MODELS	25
3.3.1 CONVECTIVE HEAT TRANSFER	25
3.3.2 THERMAL RADIATION HEAT TRANSFER	27
3.4 FLOW CORRELATIONS	28
3.4.1 COUNTERCURRENT FLOW LIMIT	28
3.4.2 REWET CORRELATION	29
3.4.3 FALLING FILM LIMIT	30
3.4.4 LIQUID ENTRAINMENT	30
3.4.5 DROPLET DRAG COEFFICIENT	31

TABLE OF CONTENTS (Continued)

	<u>Page No.</u>
4.0 BYPASS REGION MODEL	34
4.1 GOVERNING EQUATIONS	35
4.2 NUMERICAL SOLUTION TECHNIQUE	37
4.3 LIQUID DOWNFLOW THROUGH THE LOWER BYPASS JUNCTION	38
4.4 HEAT TRANSFER INTO THE BYPASS REGION	39
5.0 SUPPLEMENTARY MODELS	43
5.1 PHASE SEPARATION MODELS	43
5.1.1 DRIFT FLUX PHASE SEPARATION MODEL	43
5.1.2 WILSON BUBBLE RISE MODEL	46
5.2 UPPER PLENUM MODEL	46
5.2.1 SPRAY DROPLET ENTRAINMENT	47
5.2.2 ENTRAINMENT FROM A POOL	49
5.3 CRITICAL FLOW MODELS	49
5.4 SYSTEM DEPRESSURIZATION RATE	50
5.5 PASSIVE HEAT CONDUCTORS IN SYSTEM VOLUMES	53
5.6 EQUATION OF STATE	53
5.7 COUPLING OF THE CORE AND SYSTEM MODELS	54
5.8 SPRAY LIQUID AVAILABILITY MODEL	54
6.0 REFERENCES	61
7.0 NOMENCLATURE	64
APPENDIX A PASSIVE HEAT CONDUCTOR MODEL	A-1
APPENDIX B VERIFICATION TO FCTF DATA	B-1

LIST OF TABLES

<u>Table No.</u>		<u>Page No.</u>
3.1	BASIC CONSERVATION EQUATIONS	32

LIST OF FIGURES

<u>Figure No.</u>		<u>Page No.</u>
1.1	FLEX MODEL FEATURES	5
1.2	SAMPLE FLEX NODALIZATION FOR RECIRCULATION LINE DISCHARGE LEG BREAK	6
2.1	FLEX PIPE NODE CONTROL VOLUME	14
3.1	ILLUSTRATION OF FLEX CORE MODEL FEATURES	33
4.1	BYPASS REGION MODEL	41
4.2	BYPASS: HEAT TRANSFER FROM CHANNELS	42
5.1	FLEX DRIFT FLUX PHASE SEPARATION MODEL	57
5.2	FLEX UPPER PLENUM SCHEMATIC	58
5.3	ILLUSTRATION OF DEPRESSURIZATION MODEL	59
5.4	COUPLING OF CORE AND SYSTEM MODELS	60

1.0 INTRODUCTION AND SUMMARY

This document describes the FLEX computer code, a model developed by ENC to determine the thermal-hydraulic response during the refill and reflood phases of a Loss-of-Coolant Accident (LOCA) in a jet pump Boiling Water Reactor (BWR). FLEX complies with the NRC rules stated in 10CFR50, Appendix K⁽¹⁾. The FLEX code is used from the time of Low Pressure Core Spray (LPCS) injection into the reactor system to the time of reflood cooling; this includes the refill (filling of lower plenum with liquid) and reflood (filling of core with liquid) stages. The key result of a FLEX calculation is the time that the two-phase fluid reaches the hot node in the core (time of hot node reflood).

The FLEX code calculates this time of reflood cooling, allowing for counter-current flow phenomena and carefully accounting for the liquid inventory throughout the reactor vessel. The fate of ECCS water that is sprayed into the upper plenum is calculated as it falls by countercurrent flow through the core or bypass regions into the lower plenum. Phase separation and entrainment models are included to accurately account for liquid inventories in the reactor vessel. Break models calculate the inventory loss and depressurization rate throughout the ECCS spray period.

The principal features and capabilities of the FLEX code are illustrated pictorially in Figure 1.1, and are:

- Options for anticipated JP-BWR ECCS locations
- One dimensional hydraulic model (quasi-steady state, except for core)
- Elevated pressure and depressurization capability
- Critical flow models
- Heat transfer from vessel and internals

- Phase separation and mixture level models
- Upper plenum entrainment, from the spray and from a two-phase pool
- Two-fluid core model
- Model for the core bypass region

Best estimate models have been used in FLEX except as required by Appendix K. In the development of FLEX, the greatest modeling emphasis was placed on those regions of the reactor system where the key, controlling phenomena occur. Separate models (run simultaneously) are provided are (a) the core, (b) the bypass region, and (c) the overall reactor system where a degree of detail is consistent with importance of each region to filling the lower plenum and core with liquid.

1.1 CORE MODEL

In the core model, the rate of generation of vapor is modeled mechanistically by accounting for such phenomena as:

- Quenching of channels
- Quenching of rods
- Radiation to droplets
- Radiation to films
- Radiation to vapor
- Convection from rods to vapor
- Convection from superheated vapor to droplets
- Convection from superheated vapor to films
- Convection heat transfer between the two-phase level
- Phase changes due to heat transfer and changes in pressure
- Entrainment of liquid from the two-phase liquid level

- Countercurrent flow limiting (flooding) at the top of the core and countercurrent flow throughout the core
- Heat transfer into bypass region through the channels

The core model is applied in the active fuel region and is a two-fluid, six equation model.

1.2 BYPASS MODEL

Significant detail has also been included in the model applied to the bypass region, where the phenomena considered include:

- Heat transfer (and attendant vapor generation) from fuel channels and passive components, including quenching of the fuel channels
- Countercurrent flooding at the upper bypass junction and countercurrent flow above the liquid level
- Phase changes due to changes in pressure
- LPCI injection (plant dependent) with condensation
- One dimensional, quasi-steady flow solution

1.3 SYSTEM MODEL

The system model solves for the overall thermal-hydraulic response of the reactor system (using the core and bypass model solutions for their respective regions), and includes detailed models to account for:

- Depressurization effects
- Entrainment from the upper plenum
- Phase separation (mixture level)
- Critical flow at the break(s) (Moody or HEM)
- Heat transfer from passive components
- ECC injection at varied locations (plant dependent) with condensation

The steady state form of the evaluation model momentum equation in RELAP4⁽²⁾ is solved for the system flow solution. The transient terms not included in the FLEX momentum equation play an insignificant role in the refill and reflood phases of a LOCA. The refill and reflood phenomena are dominated by gravity (countercurrent flow) and friction effects which are included in the model.

The core, bypass and system models comprising FLEX are solved simultaneously and coupled through interfaces located at the upper and lower core boundaries, as illustrated in Figure 1.2. The network solution approach used in FLEX to obtain the system thermal-hydraulic response has been used previously by ENC in the REFLEX code⁽³⁾, which is an NRC approved model for PWR reflood licensing calculations in accordance with Appendix K. The FLEX system model is an extension of REFLEX.

1.4 APPLICATION

This document describes the models used in the FLEX code. The system solution scheme is discussed in Section 2.0, and the core and bypass models are described in Sections 3.0 and 4.0. Special model features used to account for such things as depressurization, phase separation, upper plenum entrainment, etc. are presented in Section 5.0. Appendix B of this volume contains preliminary comparisons of FLEX predictions to data from ENC's Fuel Cooling Test Facility. These comparisons strongly support the validity of the FLEX model. The results of an Example Problem application of the FLEX code to a JP-BWR refill and reflood transient are presented in Volume 2 of this document.

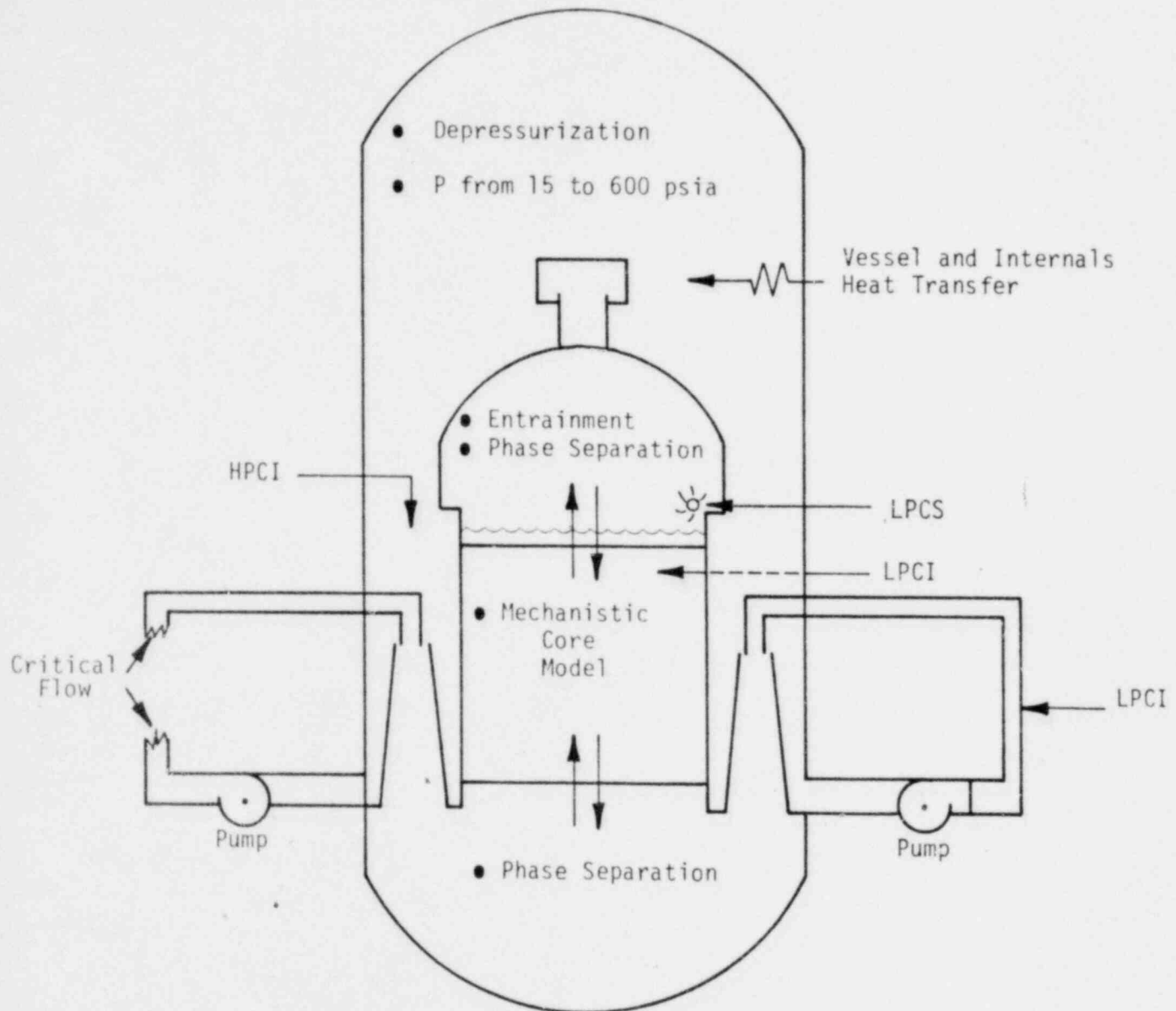


Figure 1.1 FLEX Model Features

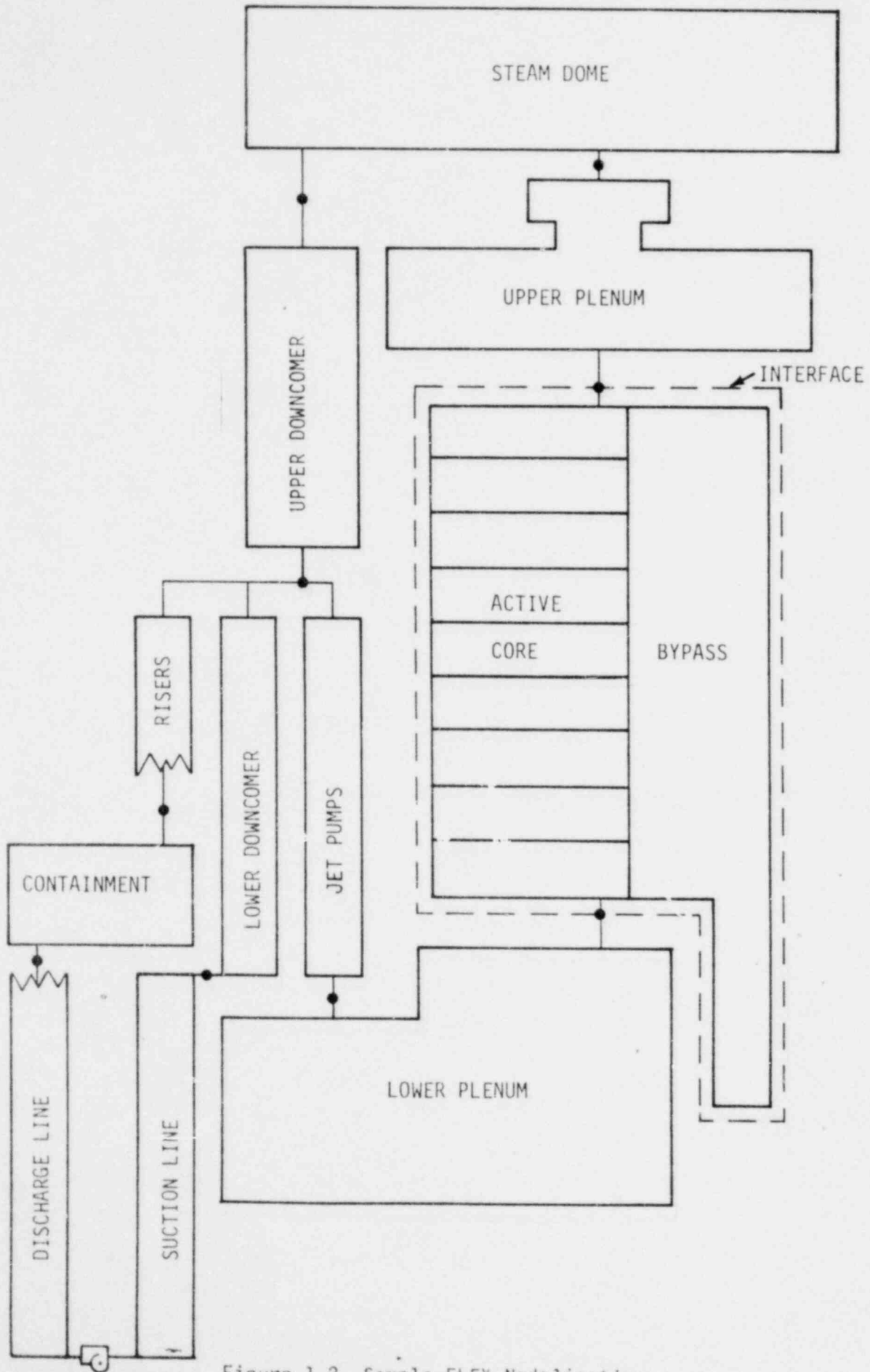


Figure 1.2 Sample FLEX Nodalization
for Recirculation Line Discharge Leg Break

2.0 FLEX SOLUTION SCHEME

This section describes the thermal-hydraulic model for the overall reactor system, exclusive of the core and bypass regions, which are treated using the models presented in Sections 3.0 and 4.0. The models are coupled at the upper and lower core boundaries as discussed in Section 5.7. The solution scheme presented in this section utilizes supplementary models which are also presented in Section 5.0. The basic solution technique has been previously used by ENC in the REFLEX code⁽³⁾, which is ENC's NRC approved licensing model for reflood analysis of PWRs.

2.1 GOVERNING EQUATIONS

The reactor system is modeled in FLEX as a combination of pipe nodes (volumes), junctions, and loops. A typical pipe node is illustrated in Figure 2.1. Mixture mass, momentum, energy and mass conservation equations are solved for each pipe node, except in the core, to obtain the change in pressure and density in each node. In the node representing the core, the equations are solved for each phase. Thermodynamic equilibrium of the phases at saturation is assumed in all FLEX nodes with the exception of the active core region, which accounts for thermodynamic nonequilibrium as described in Section 3. With this assumption, the nodal mixture temperature, quality and enthalpy are readily determined from the thermodynamic state relations describing the saturation line. Saturation properties in all nodes are evaluated at the core outlet pressure.

Junctions are the flow paths connecting nodes, and there are always two junctions for each node. Applying conservation of mass to each junction

yields a set of $J-1$ independent equations (where J is the total number of junctions used) of the form

$$\sum_j W_j = 0 \quad (2.1)$$

where W_j is either the inlet or outlet flow from the connecting nodes (depending on the reference flow direction selected by the user).

Flow loops are defined as a series of nodes, connected by junctions, around which the summation of pressure drops must equal zero. For each unchoked flow loop there is consequently an equation of the form

$$\sum_n (\Delta P)_n = 0 \quad (2.2)$$

where $(\Delta P)_n$ is the pressure drop across node n in the flow loop. The junction flow (Eq. 2.1) and loop pressure drop (Eq. 2.2) equations have been defined as recommended by Jeppsen⁽⁴⁾.

Using the convention defined in Figure 2.1, the node average flow rate, \bar{W}_n , is defined such that the node average volumetric flow rate is the average of the nodal inlet and outlet volumetric flow rates, or

$$\bar{W}_n = \frac{\bar{\rho}_n}{2} \left(\frac{W_{in,n}}{\rho_{in,n}} + \frac{W_{out,n}}{\rho_{out,n}} \right). \quad (2.3)$$

Applying the volumetric continuity equation and conservation of energy to a FLEX node undergoing a change in pressure with heat transfer, while requiring thermodynamic equilibrium of the phases, provides a second

equation set relating the nodal inlet and outlet flow rates.

$$\frac{W_{in,n}}{\rho_{in,n}} - \frac{W_{out,n}}{\rho_{out,n}} + \frac{W_{ex,n}}{\rho_{ex,n}} + \frac{v_{fg}}{h_{fg}} q_n + \frac{dP}{dt} (M_f \frac{\partial v_f}{\partial P} + M_g \frac{\partial v_g}{\partial P}) = 0 \quad (2.4)$$

where

$$q_n = q_{fill} + q_{HT} - \frac{dP}{dt} [M_f (\frac{\partial h_f}{\partial P} - v_f) + M_g (\frac{\partial h_g}{\partial P} - v_g)] + q_{sup} \quad (2.5)$$

and

$$q_{fill} = W_{fill} (h_{fill} - h_f) = \text{subcooling energy of fills.} \quad (2.6)$$

The variable q_{sup} is defined by equation 2.18 and represents the superheat energy associated with the vapor flowing out of the core region into a FLEX node. The rate of change of pressure, $\frac{dP}{dt}$, in Equations 2.4 and 2.5, is calculated as described in Section 5. The energy contribution due to heat transfer from passive structures, q_{HT} , is evaluated using the conduction model described in Section 5. The subcooling energy of fills, q_{fill} , is calculated according to Equation 2.6 assuming that the ECC injection rate and enthalpy, W_{fill} and h_{fill} respectively, are specified in the input as functions of time or pressure.

The conservation of momentum for the control volume shown in Figure 2.1 is given by:

$$dP + \frac{\rho U^2}{2} (4f \frac{dx}{D_h} + K) + \rho g dZ + \rho u du = 0 \quad (2.7)$$

which is integrated assuming constant density through the control volume to give:

$$\Delta P + \frac{\bar{W}^2}{2\rho A^2} (4f \frac{L}{D_h} + K) + \frac{1}{2\rho} \left[\frac{\bar{W}^2}{A_o^2} - \frac{\bar{W}^2}{A_i^2} \right] + \bar{\rho}g (Z_o - Z_i) = 0 \quad (2.8)$$

which is a steady state form of the momentum equation as used in the RELAP4 evaluation model. Equation 2.8 can be rearranged to give:

$$\Delta P + \bar{W}^2 K' + \bar{\rho}g (Z_o - Z_i) = 0 \quad (2.9)$$

where the equivalent loss coefficient, K' , is defined as:

$$K' = \frac{1}{2A^2 \rho} \left[4f \frac{L}{D_h} + K + A^2 \left(\frac{1}{A_o^2} - \frac{1}{A_i^2} \right) \right]. \quad (2.10)$$

The pipe wall Fanning friction factor, f , is calculated using the Karman-Nikaradse⁽⁵⁾ equation for the turbulent flow, and sixteen divided by the Reynolds Number for laminar flow. The wall friction model also uses the Baroczy two-phase multipliers⁽⁶⁾ for two-phase flow. The form loss coefficient, K , depends on the geometry and is obtained from hydraulic handbooks or from the corresponding blowdown model input.

Using Equation 2.9, the loop equations can be expressed in terms of the nodal flow rates as:

$$\sum_n [K' \bar{W}^2 + \bar{\rho}g (Z_o - Z_i)]_n = 0. \quad (2.11)$$

Conservation of mass within a pipe node is given by:

$$\frac{d\bar{\rho}}{dt} = \frac{(W_{in} - W_{out} + W_{ex})}{V} \quad (2.12)$$

where V is the node volume. Integrating (2.12) gives

$$\bar{\rho} = \bar{\rho}_0 + (W_{in} - W_{out} + W_{ex}) \Delta t \left(\frac{1}{V}\right) \quad (2.13)$$

Equations (2.13), (2.9), (2.4) and (2.3) are combined to give, for each node n :

$$\begin{aligned} \Delta P_n = & \bar{W}_n^2 K' - \rho_0 g \Delta Z - \frac{g \Delta Z \Delta t}{V} W_{ex} \\ & - \frac{g \Delta Z \Delta t}{V} \frac{\rho_{in}}{\bar{\rho}_n} \left(1 - \frac{\rho_{out}}{\rho_{in}}\right) \bar{W}_n \\ & + \frac{g \Delta Z \Delta t}{2 h_{fg} V} \frac{\rho_{in}}{\rho_g} \left(1 - \frac{\rho_g}{\rho_f}\right) \left(1 + \frac{\rho_{out}}{\rho_{in}}\right) q_n \\ & + \frac{g \Delta Z \Delta t}{2V} \frac{\rho_{in}}{\rho_{ex}} \left(1 + \frac{\rho_{out}}{\rho_{in}}\right) W_{ex} \\ & + \frac{g \Delta Z \Delta t}{2V v_{fg}} \frac{\rho_{in}}{\rho_g} \left(1 - \frac{\rho_g}{\rho_f}\right) \left(1 + \frac{\rho_{out}}{\rho_{in}}\right) \frac{dP}{dt} \left(M_f \frac{\partial v_f}{\partial P} + M_g \frac{\partial v_g}{\partial P}\right) \end{aligned} \quad (2.14)$$

and the nodal inlet and outlet flows are given by:

$$\begin{aligned} W_{in} = & \bar{W}_n \frac{\rho_{in}}{\bar{\rho}_n} - \frac{W_{ex} \rho_{in}}{2 \rho_{ex}} - \frac{v_{fg}}{h_{fg}} \frac{\rho_{in}}{2} q_n \\ & - \frac{\rho_{in}}{2} \frac{dP}{dt} \left(M_f \frac{\partial v_f}{\partial P} + M_g \frac{\partial v_g}{\partial P}\right) \end{aligned} \quad (2.15)$$

$$W_{out} = \bar{W}_n \frac{\rho_{out}}{\bar{\rho}_n} + \frac{W_{ex} \rho_{out}}{2 \rho_{ex}} + \frac{\rho_{out}}{2} \frac{dP}{dt} \left(M_f \frac{\partial v_f}{\partial P} + M_g \frac{\partial v_g}{\partial P}\right) \quad (2.16)$$

2.2 NUMERICAL SOLUTION

The junction and loop equations (2.1 and 2.2) are solved for the flow (\bar{W}_n) in each of the N nodes (N unknown \bar{W}_n 's). There is a total of $J-1$ independent junction equations.

When the break flow is not choked, N independent equations are obtained by using L loop equations where L is the number of loops ($N = J-1 + L$).

When the break flow is choked, N independent equations are obtained by using $L-1$ loop equations (the loop containing the break is not used) and one specified choked break flow. The break flows are determined by entering the choking tables (either HEM or Moody as specified by the user) with the pressure and quality in the break nodes. These choked flow values are compared to the break flows calculated, assuming that the flow is unchoked, and the lesser of the two flows is used.

The equations solved are implicit in the node average densities, $\bar{\rho}_n$. The rate of change of pressure, $\frac{dP}{dt}$, is updated iteratively during a time step using the depressurization model described in Section 5. The nodal inlet and outlet densities, which depend on $\bar{\rho}_n$, are also updated iteratively. Equations are solved by a Newton-Raphson Technique.

2.3 TREATMENT OF CORE AND BYPASS REGIONS IN SYSTEM NUMERICAL SOLUTION

A special pipe node is designated in the system model to represent the core and bypass regions. Detailed solutions for these regions are obtained using the models described in Sections 3 and 4, and the results from these models are treated as boundary conditions in the system solution scheme.

Two equations are affected. For the flow loop containing the core and bypass regions, the core pressure drop (equal to the bypass pressure drop) is defined by the core model instead of using Equation 2.14. The junction

equations containing the core and bypass flows are altered to include terms to account for the countercurrent flow and vaporization calculated by the core and bypass models.

The mass conservation equations (2.13) for the core, upper plenum, and lower plenum include the countercurrent flow (CCF) terms through the variable W_{ex} . In general, W_{ex} is defined as

$$W_{ex,n} \equiv W_{fill,n} + W_{CCF,n} + W_{ent,n} \quad (2.17)$$

where W_{fill} is the mass flow injection rate of ECC liquid, W_{CCF} is the mass flow rate of liquid into a node as restricted by CCF limitation, and W_{ent} is the mass flow rate of liquid into a pipe node by entrainment. W_{CCF} is calculated by the core at the upper boundary and by the bypass region at the upper and lower boundaries.

An additional variable supplied to the system model from the core and bypass models is the variable q_{sup} appearing in Equation 2.5, which represents the energy transport rate due to the convection of superheated vapor from the core into a FLEX node. This vapor is required to come to thermodynamic equilibrium, and consequently gives up energy at the rate

$$q_{sup,n} = W_{sup,n} (h_{sup,n} - h_g) \quad (2.18)$$

where $h_{sup,n}$ is the superheated vapor enthalpy and $W_{sup,n}$ is the mass flow rate of superheated vapor into node n .

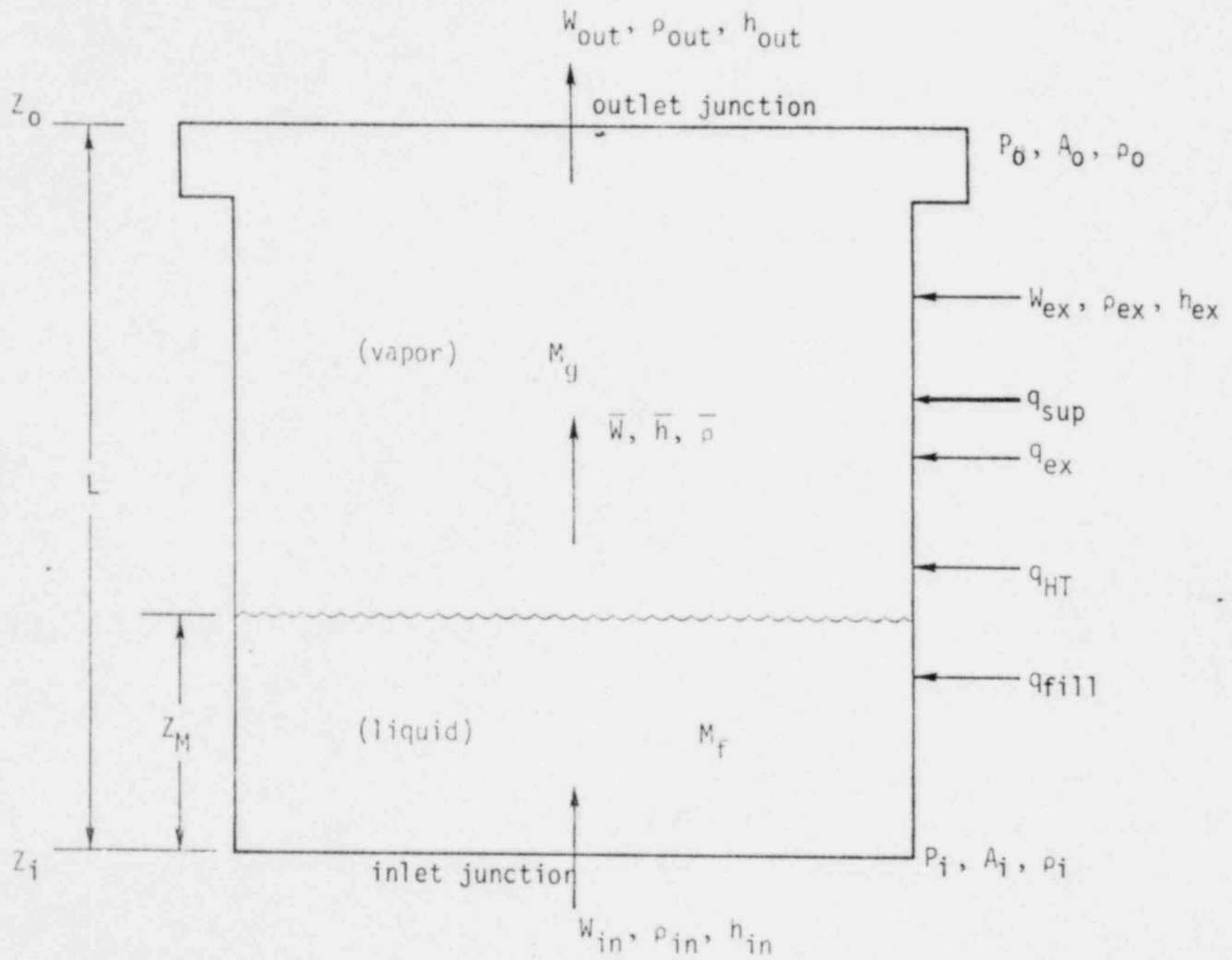


Figure 2.1 FLEX Pipe Node Control Volume

3.0 FLEX CORE MODEL

The core model was developed to evaluate BWR core performance during a period characterized by ECCS injection, countercurrent flow, depressurization and reflood. Appendix B provides a preliminary verification of the core model by comparing FLEX predictions to ENC Fuel Cooling Test Facility spray and reflood test data; the conservative FLEX prediction of the time of hot node reflood is demonstrated.

3.1 THE PHYSICAL PHENOMENA

During the refill period of a loss of coolant accident, the reactor system is depressurizing, and the flow accelerations have diminished. This period of the transient is characterized by countercurrent, dispersed flow and falling film rewetting in the core during which time the lower plenum is accumulating liquid. When the lower plenum fills to the lower core boundary, reflooding of the core begins (see Figure 3.1) which rapidly terminates the fuel temperature rise (PCT turnaround), and a two-phase mixture progresses upward through the core. Entrainment and countercurrent dispersed flow are modeled above the two-phase mixture level as shown in Figure 3.1.

The core model evaluates the key phenomena that contribute to the vaporization rate in the core. Because of countercurrent flow limitations at the upper tie plates, this vaporization rate, together with the vapor flow from the lower plenum, controls the rate at which the liquid can penetrate downward through the upper tie plate and the core to the lower plenum.

The key features of the FLEX core model include:

- Two-fluid, six equation thermal-hydraulic model
- Thermodynamic nonequilibrium accounted for (vapor superheat in presence of saturated liquid) above the two-phase mixture level

- Rod and channel to vapor convective heat transfer
- Rod and channel to liquid film convective heat transfer
- Vapor to liquid film convective heat transfer
- Vapor to droplet convective heat transfer
- Two-dimensional radiation heat transfer, for as many as 65 different surfaces (8x8 rod array and a channel), assuming gray and diffuse surfaces and non-scattering media
- Radiant rod and channel to rod heat transfer
- Radiant rod and channel to vapor heat transfer
- Radiant vapor to droplet heat transfer
- Quenching and rewetting of rods and channel (rates may be limited by temperature, liquid availability, or by film velocity)
- Countercurrent flow limiting at top of core
- Two-phase mixture level progress through core during reflood
- Liquid entrainment from the two-phase mixture level during reflood.

The core model considers one average vertical thermal-hydraulic flow channel per fuel assembly and has the capability to consider more than one rod type in a fuel assembly.

3.2 CONSERVATION EQUATIONS

Six conservation equations plus the state and interphase relations are used to describe the two-phase dispersed flow region. Two equations are used to conserve mass in the vapor and liquid phases. Two momentum equations define the effect of the interfacial forces on the dispersed droplet phase, and the spacial pressure gradients of the combined phases. An energy equation

describes the vaporization rate from the droplet phase due to depressurization and heat transfer. Since thermodynamic nonequilibrium is allowed in the core region, the second energy equation is used to characterize the vapor superheat. The basic constant-property one-dimensional conservation equations in classical form⁽⁵⁾ are summarized in Table 3.1 for the two-phase dispersed flow region. The subsections herein modify the conservation equations to the form actually solved in FLEX and present the associated constitutive relations.

Thermodynamic nonequilibrium is allowed in the form of superheated vapor in conjunction with saturated liquid only. Subcooled liquid alone or in the presence of vapor is not allowed. The depressurization rate is determined by the method described in Section 5.4 and is applied as a boundary condition to the energy conservation equations.

The rewet films are assumed to be of uniform thickness and their progression is limited by either a conduction based rewet correlation, by liquid availability, or by momentum considerations. Consequently two conservation equations are sufficient to describe their actions. A liquid energy equation, equivalent to that used in the dispersed flow region, governs the vapor generation rate, and a mass conservation equation determines the excess liquid available at the rewet location.

In the continuous liquid region below the mixture level, assumptions of thermodynamic equilibrium and a void fraction that is linear from the bottom of the core to the liquid level reduces the number of required conservation equations to three. These are conservation of the mixture mass, the energy equation defining the rate of phase change, and the momentum mixture equation which defines the pressure differentials.

3.2.1 Conservation of Mass

The conservation of mass equation in Table 3.1 for vapor flow in the dispersed flow region can be written as,

$$\rho_v \frac{\partial \alpha_v}{\partial t} + \alpha_v \frac{\partial \rho_v}{\partial t} + \frac{\partial}{\partial z} (\alpha_v \rho_v u_v) = \sum_i \Gamma_{i,v} + S_v \quad (3.1)$$

where i indicates the droplet or film phase. Γ_v is the vaporization rate and S_v is any other source of vapor. α_v is the void fraction (same as α). The partial derivative $\frac{\partial \rho_v}{\partial t}$ can be written as

$$\frac{\partial \rho_v}{\partial t} = \frac{\partial \rho_v}{\partial P} \frac{dP}{dt} \quad (3.2)$$

The rate of change of pressure, $\frac{dP}{dt}$, is taken as a boundary condition. It is assumed that the density of the vapor is at saturated conditions, and the rate of change in vapor density is described in Equation 3.2, with the derivative $\frac{\partial \rho_v}{\partial P}$ determined following the saturation line. Equation 3.1 shows that the vapor mass flow rate increases spatially according to the rates of vaporization, displacement, and expansion.

Continuity of the film mass determines the excess liquid available ($W_{f,d}$) at the rewet fronts.

$$W_{f,d} = S_f - \Gamma_{f,v} + A_{f,d} \rho_f u_q \quad (3.3)$$

where u_q is the quench front velocity. The excess liquid at the rewet front is a source of droplets.

The droplets are conserved in both mass and number. The relationship governing the change in droplet mass from Table 3.1 is,

$$\rho_d \frac{\partial \alpha_d}{\partial t} + \rho_d \frac{\partial (\alpha_d u_d)}{\partial z} = S_d - \Gamma_{d,v} \quad (3.4)$$

where α_d is the volumetric fraction of droplets, (droplet fraction which = $1-\alpha$), and $\Gamma_{d,v}$ is the vaporization rate of droplets. The relation defining the change in number density of the droplets is,

$$\frac{\partial n_d}{\partial t} = \frac{\partial}{\partial z} (u_d n_d) + n_d \quad (3.5)$$

where

$$n_d = \frac{6 S_d}{\pi \rho_d d_d^3} \quad (3.6)$$

The variable d_d is the droplet formation diameter corresponding to the source S_d .

During reflood, the void fraction below the mixture level is assumed to vary linearly with height.

$$\alpha_v = \frac{\gamma z}{y}$$

where γ is the void fraction at the mixture level and y is the mixture level.

Conservation of liquid and vapor masses in this region determines the rate at which the mixture level rises,

$$\frac{dy}{dt} = \frac{2}{(2-\gamma) A \rho_f} \left(A \int_0^y S_k dy - A \int_0^y \Gamma_{\ell,v} dy + W_{\ell 0} - W_{\ell/y} \right), \quad (3.8)$$

and the rate of vapor flow relative to the moving mixture level,

$$W_{v/y} = A \int_0^y \Gamma_{\ell,v} dy + A \int_0^y S_v dy - \frac{A \gamma \rho g}{z} \frac{dy}{dt}. \quad (3.9)$$

Equations 3.7, 3.8 and 3.9 and a momentum relation for the relative velocity of the liquid with respect to the interface ($W_{\ell/y}$) are solved simultaneously.

3.2.2 Conservation of Energy

The energy conservation equation in Table 3.1 defining the vapor superheat can be rewritten as:

$$\begin{aligned} \frac{\partial h_v}{\partial t} + \frac{1}{\alpha_v A \rho_v} \frac{\partial}{\partial z} (W_v h_v) &= \frac{h_v}{\alpha_v \rho_v A} \frac{\partial}{\partial z} (W_v) \\ &+ \frac{q_v}{\alpha_v \rho_v} + \frac{1}{\rho_v} \frac{dP}{dt} + \frac{\sum_i \Gamma_{i,v}}{\alpha_v \rho_v} (h_g - h_v). \end{aligned} \quad (3.10)$$

The form of Equation 3.10 is consistent with the donor cell logic used within the program.

Vaporization rates of liquid in the presence of superheated vapor are defined to be

$$\Gamma_{i,v} = - \frac{\alpha_i \rho_i \frac{dP}{dt} \frac{dh_f}{dP} - u_f}{h_{fg}} + \frac{q_i}{h_{fg}}, \quad i = f, d, \ell. \quad (3.11)$$

This equation defines the rate of phase change for both the droplet and film fields. When applied in reflood to the region below the mixture level in the core (subscript λ) the depressurization term is assumed negligible and ignored. Since both phases below the mixture level are assumed to be saturated, one energy equation is sufficient in this region.

3.2.3 Conservation of Momentum

The droplet momentum equation of Table 3.1 can be written in detail as

$$\alpha_d \rho_d \frac{\partial u_d}{\partial t} + \alpha_d \rho_d u_d \frac{\partial u_d}{\partial z} = S_d (u_d^* - u_d) + F_d - \alpha_d \rho_d g, \quad (3.12)$$

where u_d^* is the velocity of the droplet source S_d . The axial pressure gradient term does not appear as it is negligible compared to gravity in this discontinuous droplet phase. The interphase force between the droplets and the vapor is determined by

$$F_d = n_d \frac{\pi}{4} d_d^2 C_D \frac{1}{2} \rho_v |u_d - u_v| (u_d - u_v), \quad (3.13)$$

where C_D is the drag coefficient described in Section 3.4.5.

The continuous phase vapor momentum equation is reduced from Table 3.1 in a similar manner and can be written as:

$$\frac{\partial P}{\partial z} = -\rho_v u_v \frac{\partial u_v}{\partial z} + \frac{F_v}{\alpha_v} - \rho_v g + \frac{1}{\alpha_v} \sum_i \Gamma_{i,v} (u_i - u_v). \quad (3.14)$$

The temporal acceleration term and compressibility terms are not included as they are negligible in this quasi steady state refill period.

The four terms governing the pressure gradient are the spacial accelerations, the frictional interactions with the droplets and the other surfaces, the body forces, and the exchange of momentum due to phase changes. At the tieplates additional pressure differentials are calculated to be

$$\Delta P = \frac{K \rho_v u_v^2}{2} \quad (3.15)$$

where the loss coefficient is taken from hydraulic test results.

An approach suggested by Wallis⁽⁹⁾ is used to define the pressure differential below the mixture level, where the pressure gradient is formed by the sum of three contributions: the frictional part, the spacial acceleration component, and that due to body forces,

$$\frac{dP}{dz} = \left(\frac{dP}{dz} \right)_F + \left(\frac{dP}{dz} \right)_A + \left(\frac{dP}{dz} \right)_G \quad (3.16)$$

The frictional portion is defined as

$$\left(\frac{dP}{dz} \right)_F = -2 C_F \rho_m \frac{u_m^2}{D_h} \quad (3.17)$$

Defining $\rho_m = \frac{yZ}{y} \rho_g + (1 - \frac{yZ}{y}) \rho_f$, integrating from 0 to y, and using the assumption of equation (3.7) yields;

$$(P_y - P_0)_F = \frac{C_F y}{D_h} \frac{|W_{f0}| W_{f0}}{\left[\frac{y}{2} \rho_g + (1 - \frac{y}{2}) \rho_f \right] A^2} \quad (3.18)$$

The spacial acceleration portion of Equation 3.16 is.

$$\left(\frac{dP}{dz} \right)_A = - \frac{W}{A} \frac{du}{dz} \quad (3.19)$$

Ignoring the effect of the control volume changing size, the spacial acceleration can be integrated from 0 to y to yield:

$$(P_y - P_0)_A = \frac{1}{2A} (-\rho_g u_g^2|_y - \rho_f u_k^2|_y + \rho_f u_k^2|_0) \quad (3.20)$$

The remaining gravitational contribution is,

$$\left(\frac{dP}{dz} \right)_G = - \rho_m g \quad (3.21)$$

Performing the integration and using equation (3.6) yields,

$$(P_y - P_0)_G = - \left[\frac{\gamma \rho}{2} + (1 - \frac{\gamma}{2}) \rho_k \right] g y \quad (3.22)$$

The total pressure difference is then,

$$P_y - P_0 = (P_y - P_0)_F + (P_y - P_0)_A + (P_y - P_0)_G \quad (3.23)$$

The only undefined parameter is the friction loss coefficient, C_F . Wallis⁽⁹⁾ reports 0.005 to be a reasonable coefficient for turbulent flow.

3.2.4 Heat Transfer From Solid Components

In the channel, the temperature gradients are negligible except in the neighborhood of a film front, and the energy conservation given by the stored energy lumped relation is:

$$\frac{dT_c}{dt} = \frac{-\sum_i q'_c i}{\rho_c C_p 4(X-\delta_c)\delta_c} \quad (3.24)$$

The heat flux per unit length, q'_c , is defined on the interior and the exterior of the channel to be positive away from the surface. X is the outside dimension of channel.

The temperatures within the fuel rod are determined by a finite difference approximation to the one dimensional transient conduction equation in cylindrical coordinates,

$$\rho C_p \frac{\partial T}{\partial t} = k \frac{\partial}{\partial r} \left(\frac{1}{r} \frac{\partial T}{\partial r} \right) \quad (3.25)$$

subjected to the boundary conditions imposed by convection and radiation.

3.3 HEAT TRANSPORT MODELS

Energy balances and correlations are used to define the rate of transport of thermal energy between mediums. Included are convection from the surfaces to the fluid phases, convection between the phases, conduction limited quenching models, and radiation in an enclosure with participating media.

3.3.1 Convective Heat Transfer

The core model considers four convective heat transfer components. They are:

- ° surface to vapor
- ° surface to film
- ° vapor to film
- ° vapor to droplets

The surface to vapor and vapor to film paths are both governed by the Dittus Boelter relation⁽⁸⁾,

$$\text{Nu} = 0.023 \text{ Re}^{0.8} \text{ Pr}^{0.4} \quad (3.26)$$

The lower limit of the Nusselt number is 4. This is a mean of the values for constant heat flux and constant wall temperature heat transfer in laminar flow.

The relation governing the rate of heat convected between the vapor and droplet phase is,

$$Nu_d = 2.0 + 0.6 Re_d^{0.5} Pr_v^{0.33} \quad (3.27)$$

This relation is reported accurate for Reynolds numbers, based on the droplet diameter, of less than 2000 (10), which is the anticipated range of droplet Reynolds Numbers.

For a film covering a wetted surface the convective coefficient is considered infinite. The heat transfer per unit length of surface becomes the sum of any decay power per unit length and a contribution due to changing saturation temperature;

$$q'_f = p' - \rho_f C_{pf} A \frac{dT_s}{dp} \frac{dP}{dt} \quad (3.28)$$

Below the mixture level the convective coefficient is taken from the modified Bromley pool film boiling correlation (11).

3.3.2 Thermal Radiation Heat Transfer

Superimposed on the transport of thermal energy by convection is the transport due to radiation. The equations describing radiation within an enclosure are developed in general by Siegel and Howell⁽¹²⁾. These have been extended to a rod bundle geometry containing two participating mediums, vapor and droplets, and the resulting matrix is

$$\sum_j \left[\delta_{i,j} - (1-\epsilon_i) F_{ij} \tau_{ji} \right] B_j = \epsilon_i E_i + (1-\epsilon_i) \sum_j (F_{ij} \epsilon_{gij} E_g + F_{ij} \epsilon_{dij} E_d) \quad (3.29)$$

where δ_{ij} is the Kronecker delta. Radiation in the axial direction is assumed negligible.

If a_d is the absorptance of the droplet phase without the presence of vapor, and a_v is the absorptance of the vapor phase without droplets, the geometric-mean transmittance, τ_{ij} , is

$$\tau_{ij} = (1-a_{dij}) (1-a_{vij}). \quad (3.30)$$

The emittance, ϵ_{gij} , is the emittance of the vapor in a vapor droplet mixture, and the emittance, ϵ_{dij} , is the emittance of the droplets in a vapor droplet mixture.

The matrix of equations, 3.29, is applicable to any two dimensional radiation problem within an enclosure subject to the restrictions of the assumptions that the surfaces are gray and diffuse, and the participating media are nonscattering. When applied to fuel assemblies the FLEX radiation model can treat as many as 65 surfaces (an 8x8 rod array within a channel).

When one rod type is considered in FLEX, the complete 64 rod (plus channel) radiation matrix is calculated, assuming all rods are the same temperature to obtain the net radiation to vapor, droplets and channel.

3.4 FLOW CORRELATIONS

In special instances, local flow conditions are described by correlations which are substituted for the detailed momentum and continuity correlations. Such correlations are used to determine the countercurrent flow limit (CCFL) at the top of the fuel assembly, film progression when conduction is limited, the maximum rate at which a film can fall when not limited by quenching or by liquid availability, and to describe the rate of liquid entrainment from the mixture level while the core is reflooding.

3.4.1 Countercurrent Flow Limit

The countercurrent flow limit (CCFL) phenomenon is modeled in FLEX using a correlation based on the Kutateladze numbers^(14,15):

$$\sqrt{K_g} + \sqrt{-K_f} = 1.79 \quad (3.31)$$

where the Kutateladze numbers are,

$$K_g = \left\{ \rho_g j_g / [g \sigma (\rho_f - \rho_g)] \right\}^{\frac{1}{2}} \left\{ \frac{1}{2} \right\} \quad (3.32)$$

and

$$K_f = \left\{ \rho_f j_f / [g \sigma (\rho_f - \rho_g)] \right\}^{\frac{1}{2}} \left\{ \frac{1}{2} \right\} \quad (3.33)$$

where σ is the surface tension.

3.4.2 Rewet Correlation

A rewet correlation valid for relatively thick or thin materials is used to describe the rate of rewet or quenching. The correlation from Anderson⁽¹³⁾ is:

$$Pe = \left[\left(\frac{\sqrt{Bi}}{\theta} \right) + 2 \frac{-3\sqrt{\pi}}{4} \left(\frac{Bi}{\theta \cdot 1.886} \right) \right]^{\frac{1}{3}} \quad (3.34)$$

and the non-dimensional numbers are:

$$Pe = \rho_w C_w (-u_q) \delta_w \quad (3.35)$$

$$Bi = \frac{h_{fr} \delta_w}{k_w} \quad (3.36)$$

$$\theta = \left[\frac{(T_w - T_s)(T_w - T_o)}{(T_o - T_s)^2} \right]^{\frac{1}{2}} \quad (3.37)$$

The core model assumes $T_w = T_s + 50 \text{ C}^0$, and h_{fr} was taken from experimental data as $175,000 \text{ W}/(\text{m}^2 \cdot \text{C}^0)$ for the fuel rods, and $1.46 \times 10^6 \text{ W}/(\text{m}^2 \cdot \text{C}^0)$ for the channel.

3.4.3 Falling Film Limit

Wallis⁽⁹⁾ presents an equation for the mass flow per unit width for a falling film in annular flow when the interfacial shear stresses and pressure drop are negligible. For a film thickness δ_f the mass flow per unit width is,

$$w_f = \frac{\rho_f \delta_f^3 g (\rho_f - \rho_v)}{3\mu} \quad (3.38)$$

Equation (3.38) is used as a limit for the falling films if they are not limited by rewet correlations or liquid availability. Normally one of the latter two phenomena are limiting.

3.4.4 Liquid Entrainment

The rate at which liquid is entrained from the mixture level into the dispersed flow region is defined by a correlation of Weber numbers⁽¹⁶⁾. The relation defines a fraction which is the ratio of entrainment rate to liquid upflow rate available at the mixture level. The entrainment fraction, ψ , is linear in terms of Weber number between onset of entrainment (We_{oe}) and the point of total entrainment (We_{Te}).

$$\psi = \frac{We - We_{oe}}{We_{Te} - We_{oe}} \quad (3.39)$$

The Weber number is,

$$We = \frac{\rho_g (u_g - u_l)^2 D_h}{\sigma} \quad (3.40)$$

3.4.5 Droplet Drag Coefficient

The droplets are assumed to be spherical in form. Drag coefficients for flow over spheres are generally presented as a function of Reynolds number ⁽¹⁷⁾. Within the FLEX core model, the drag coefficient is approximated by,

$$C_d = 0.4 + 25.4 \text{ Re}_d^{-0.8} \quad (3.41)$$

TABLE 3.1

BASIC CONSERVATION EQUATIONS
(Continuous Vapor and Dispersed Droplets)

MASS

$$\text{Vapor:} \quad \frac{\partial(\alpha\rho_v)}{\partial t} + \frac{\partial(\alpha\rho_v u_v)}{\partial z} = \text{vapor source}$$

$$\text{Droplets:} \quad \frac{\partial((1-\alpha)\rho_d)}{\partial t} + \frac{\partial((1-\alpha)\rho_d u_d)}{\partial z} = \text{droplet source}$$

MOMENTUM

$$\text{Vapor:} \quad u_v \frac{\partial u_v}{\partial z} = -\frac{1}{\rho_v} \frac{\partial P}{\partial z} - g + \text{friction} + \text{source}$$

$$\text{Droplets:} \quad \frac{\partial u_d}{\partial t} + u_d \frac{\partial u_d}{\partial z} = -g + \text{friction} + \text{source}$$

ENERGY

$$\begin{array}{l} \text{Vapor:} \\ \text{(Superheat)} \end{array} \quad \frac{\partial T_v}{\partial t} + u_v \frac{\partial T_v}{\partial z} = \text{convection} + \text{source} + \text{work}$$

$$\begin{array}{l} \text{Droplets:} \\ \text{(Saturated)} \end{array} \quad h_{fg} (\text{vaporization rate}) = \text{convection} + \text{source}$$

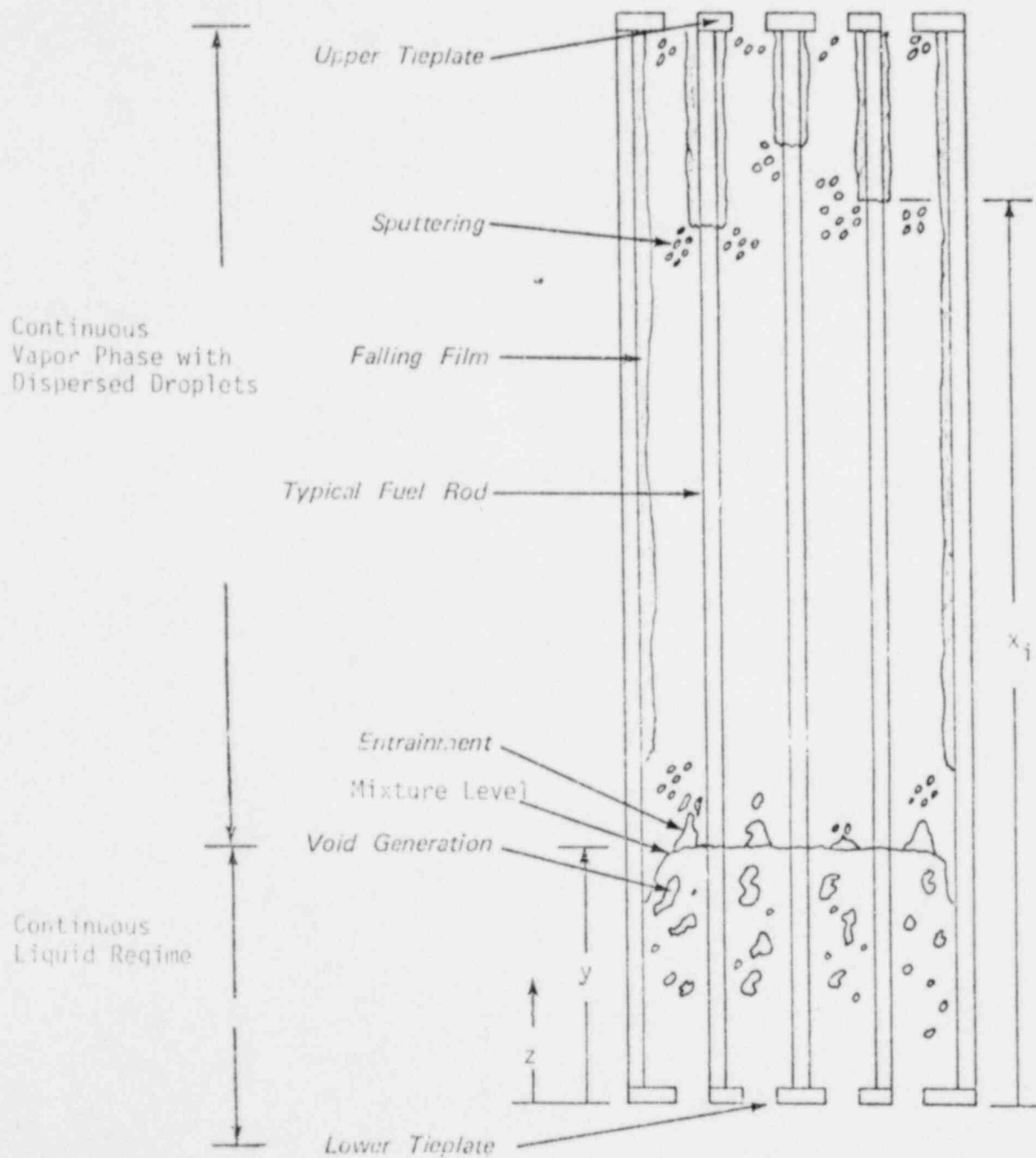


Figure 3.1 Illustration of FLEX Core Model Features

4.0 BYPASS REGION MODEL

The bypass region is defined to consist of the guide tubes and all the space inside the core shroud, but outside the fuel channels. The bypass region provides an important path for ECCS liquid to reach the lower plenum. The bypass and core models are solved simultaneously subject to the requirement of equal pressure drops.

The FLEX bypass model solves the momentum, continuity, and energy equations, and considers the following phenomena:

- Countercurrent flow limitation at the upper bypass junction
- Condensation due to subcooled ECC injection
- Phase changes due to changes in pressure (flashing)
- Liquid level within the bypass region
- Heat transfer from passive components
- Heat transfer through the channels (from the fuel assemblies)
- Quenching of the channels
- Countercurrent flow above the liquid level in the bypass, including determination of the void fraction above the liquid level
- Liquid penetration through the bypass into the lower plenum
- LPCI for appropriate plants

The results from the bypass model calculations are the liquid and vapor mass flow rates into both the upper and lower plenums. While countercurrent flow is considered at the upper junction, single phase flow (steam or liquid only)

is considered at the lower bypass junction which communicates with the lower plenum. No liquid is permitted to pass from the bypass into the lower plenum until the guide tubes have filled.

4.1 GOVERNING EQUATIONS

With the assumption of thermodynamic equilibrium of the phases, one of the three basic governing equations of the bypass model is obtained by combining the conservation of mass and energy equations for the bypass volume shown in Figure 4.1 to yield

$$\begin{aligned} & (W_{f\ell} - W_{fu} + W_{LPCI})v_f + (W_{g\ell} - W_{gu})v_g \\ & = \frac{v_{fg}}{h_{fg}} \left\{ \frac{dP}{dt} \left[M_f \left(\frac{\partial h_f}{\partial P} - v_f - \frac{h_{fg}}{v_{fg}} \frac{\partial v_f}{\partial P} \right) + M_g \left(\frac{\partial h_g}{\partial P} - v_g - \frac{h_{fg}}{v_{fg}} \frac{\partial v_g}{\partial P} \right) \right] \right. \\ & \quad \left. - q_h - q_c - q_{LPCI} \right\}. \end{aligned} \quad (4.1)$$

Equation 4.1 gives the relationship between the flows into and out of the bypass ($W_{f\ell}$, W_{fu} , $W_{g\ell}$, W_{gu} , W_{LPCI}), the energy transport into the bypass (q_h , q_{HT} and q_{LPCI}), and the effects of pressure changes within the bypass (phase changes and changes in specific volumes of the phases due to changes in pressure). The energy transport terms are defined in Figure 4.1, and q_c includes the energy conducted from the fuel assembly through the channel wall (q_{bc}) as well as from other metal components.

The second governing equation in the bypass is the momentum equation, written in the quasi-steady form of the system loop equations. The insignificant transient terms are ignored, leaving the dominant terms for a refill/reflood transient:

$$\Delta P_{\text{bypass}} = \Delta P_{\text{friction,form}} + \Delta P_{\text{gravity}} \quad (4.2)$$

Referring to Figure 4.1, it can be seen that three distinct regions can exist between the upper and lower junctions where the pressure drop boundary condition is applied: a liquid region (between Z_ℓ and Z_L), a region between the falling film quench front and the liquid (between Z_q and Z_L , called Region B) and Region T which contains the films on the channels. The gravity terms are:

$$\begin{aligned} \Delta P_{\text{gravity}} = & -g (Z_L - Z_\ell) \rho_f - g (Z_q - Z_L) [\alpha_B \rho_g + (1 - \alpha_B) \rho_f] \\ & - g (Z_u - Z_q) [\alpha_T \rho_g + (1 - \alpha_T) \rho_f] \end{aligned} \quad (4.3)$$

The friction and form losses considered are:

$$\begin{aligned} \Delta P_{\text{friction, form}_u} = & -K_u \frac{1}{2A_u^2} \left[\frac{|W_{fu}| W_{fu}}{\rho_f} + \frac{|W_{gu}| W_{gu}}{\rho_g} \right] \\ \Delta P_{\text{friction, form}_\ell} = & -K_\ell \frac{1}{2A_\ell^2} \left[\frac{|W_{f\ell}| W_{f\ell}}{\rho_f} + \frac{|W_{g\ell}| W_{g\ell}}{\rho_g} \right]. \end{aligned} \quad (4.4)$$

The friction losses through the lower bypass junction are by far the dominant term in Equation 4.4.

The void fractions (α_B and α_T) appearing in Equation 4.3 are calculated assuming steady state flows of liquid and vapor above the liquid level (w_{fu} and w_{gu}). The relative velocity of the droplets and vapor are calculated assuming that all droplets have a size corresponding to a Weber (We) number of $12.0^{(9)}$, and the drag coefficient (C_D) is consistent with Equation 3.41.

$$U_R = \left(\frac{4We}{3C_D} \right)^{1/4} \left[\frac{\sigma(\rho_f - \rho_g)g}{\rho_g^2} \right]^{1/4}. \quad (4.5)$$

Using this relative velocity U_R and the flow rates of the phases, the void fraction is given by the appropriate root of

$$\alpha_B^2 (\rho_f \rho_g A_b U_R) + \alpha_B (-\rho_g W_f - \rho_f W_g - \rho_f \rho_g A_b U_R) + \rho_f W_g = 0. \quad (4.6)$$

The void fraction in the top region (α_T) is also computed using Equation 4.6 but includes the contribution of the liquid films on the outside of the channels.

The third (and final) governing equation in the bypass region is the countercurrent flow relationship at the upper bypass junction, which gives the dependence of liquid downflow on vapor upflow. The Kutateladze correlation is used (Equation 3.31).

4.2 NUMERICAL SOLUTION TECHNIQUE

Equations 4.1, 4.2 and 3.31 are the three governing equations solved simultaneously to obtain the flows into and out of the bypass. Because the flow at the lower bypass junction is assumed to be either vapor or liquid, but not both, three equations are sufficient to uniquely solve for the three unknown flow rates ($W_{f\ell}$ or $W_{g\ell}$, W_{fu} and W_{gu}).

The bypass equations are solved simultaneously with the core model during a time step, subject to the assumption of equal pressure drop across the core and the bypass. Solving the bypass equations is a simple three step, non-iterative process. The inlet flow is first specified, and Equation 4.1 is solved for the net volumetric flow (Q_{net}) required at the upper bypass junction. The liquid and vapor mass flow rates, W_{fu} and W_{gu} , at the upper junction are then solved for using the relation

$$Q_{net} = W_{fu} v_f + W_{gu} v_g \quad (4.7)$$

and the countercurrent flow limiting correlation, Equation 3.31, subject to the restriction that W_{fu} can not exceed the liquid availability limit (see Section 5). Once all the flows are known, the bypass pressure drop is readily evaluated according to Equations 4.2, 4.3 and 4.4.

4.3 LIQUID DOWNFLOW THROUGH THE LOWER BYPASS JUNCTION

This flow path consists of numerous leakage paths, in addition to the flow paths afforded by the alternate bypass flow holes (in the lower tie plate sidewalls of the fuel assemblies) and the reverse flow leakage path between the lower tie plates and the fuel channels. The liquid level in the bypass region will, during the course of a typical refill/reflood transient, become sufficiently high to push liquid through these leakage paths (lower bypass junction) into the lower plenum.

For this special case, the friction losses through the lower bypass junction are described using a correlation developed by the BWR NSSS vendor⁽¹⁹⁾, which has been modified by ENC to account for the lower tie plate to channel leakage path and the alternate bypass flow holes in the lower tie plate walls:

$$W_{fL} = \beta_1 \Delta P^{1/2} + \beta_2 \Delta P + \beta_3 \Delta P^2 \quad (4.8)$$

where W_{fL} is in units of lb_m/hr , and ΔP is in units of lb_f/in^2 , and the coefficients β_1 , β_2 and β_3 are described by

$$\beta = 2814 N_{gt} + 11660 N_h + 101.4 N_{inst} + 6.86 N_b + 272200 \rho_f^{1/2} \left[\sum_{i=1}^{N_{ft}} (D_{abfh,i}^2 K_{abfh,i}^{1/2} N_{abfh,i}) \right] + 14966 + \delta_i$$

$$\beta_2 = -70.07 N_{gt} - 8.61 N_{inst} + 15.55 N_b + 1084$$

$$\beta_3 = 1.952 N_{gt} + 0.2 N_{inst} - 0.058 N_b - 12.3$$

N_{ft} = number of different fuel types in core

N_{gt} = number of guide tubes

N_h = number of core plate holes

N_{inst} = number of instrument tubes

N_b = total number of fuel bundles in core

$N_{abfh,i}$ = number of alternate bypass flow holes in fuel type i

$D_{abfh,i}$ = diameter of alternate bypass flow holes in fuel type i

$K_{abfh,i}$ = loss coefficient for reverse flow through alternate flow holes in fuel type i

δ_i = term to account for leakage flow through the lower tie plate to channel seal for fuel type i .

No liquid downflow is permitted through the lower bypass junction until the liquid level in the bypass region has covered the lower bypass junction. It is to be noted that this criterion requires that the guide tubes be filled before any liquid is allowed to flow into the lower plenum from the bypass.

4.4 HEAT TRANSFER INTO THE BYPASS REGION

Heat transfer into the bypass region is considered from both passive components (e.g., core shroud, guide tubes, etc.) and from the fuel channels. The passive components are treated using the model described in Section 5.

The fuel channels are subdivided into axial segments, as illustrated in Figure 4.2. For any axial node not containing the quench front, the heat transfer rate is calculated by the relation

$$q_i = h A_{si} (T_{wi} - T_{sat}) \quad (4.9)$$

where h = heat transfer coefficient (see Section 5.5)

A_{si} = surface area of node i

T_{wi} = wall temperature of node i

For the node containing the quench front, the heat transfer rate is computed only for the region beneath the quench front as given by

$$q_i = \frac{(Z_q - Z_i)}{\Delta Z_i} h A_{si} (T_{wi} - T_{sat}) \quad (4.10)$$

The total heat transfer rate into the bypass from the channels is thus described by

$$q_{bc} = \sum_i q_i + q_q + q_{film} \quad (4.11)$$

where q_q is the total quench front heat transfer rate provided to the bypass model from the core model, and q_{film} is the heat transfer rate required to hold the quenched portions of the channels at saturation temperature as pressure is changing.

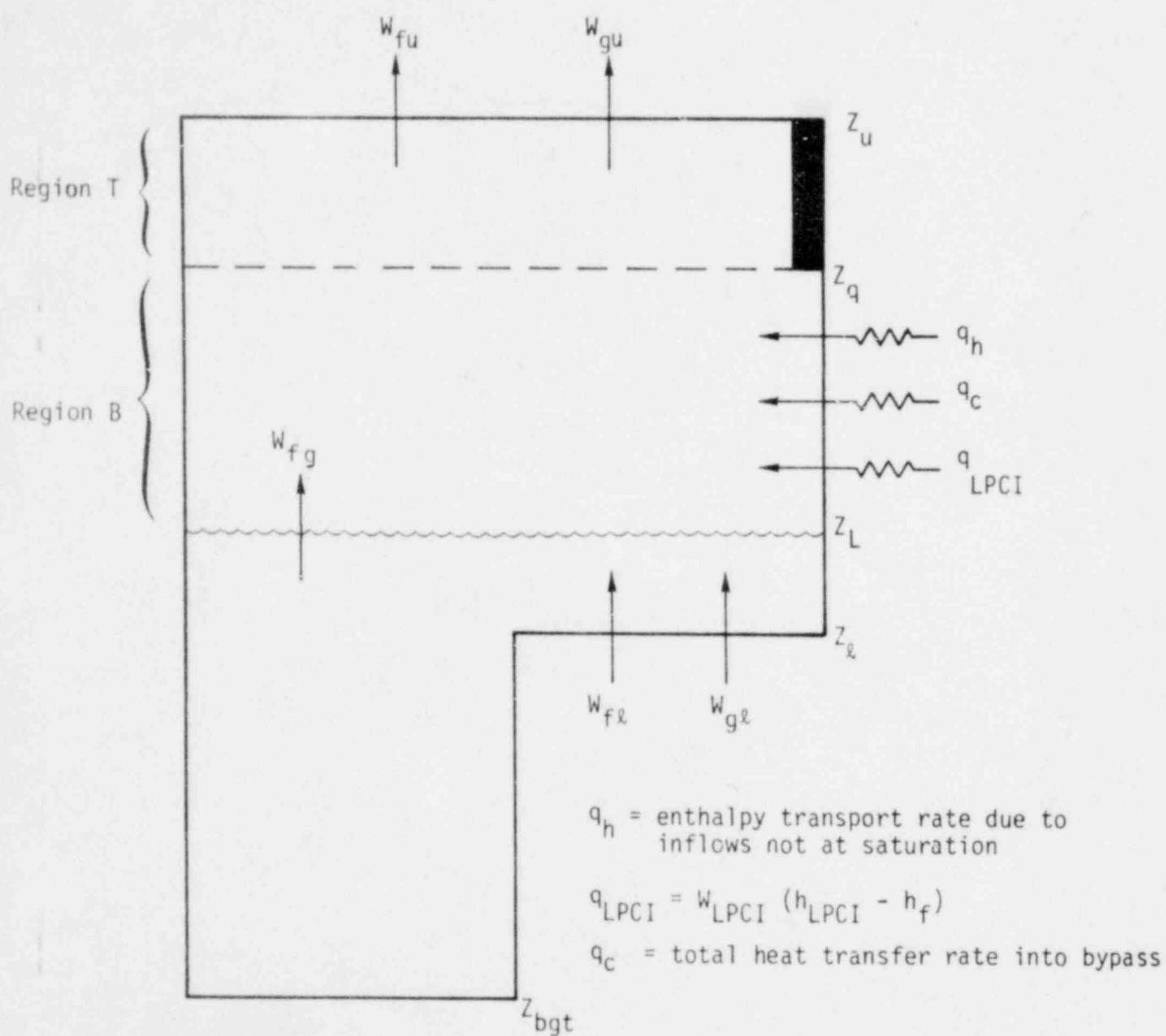


Figure 4.1 Bypass Region Model

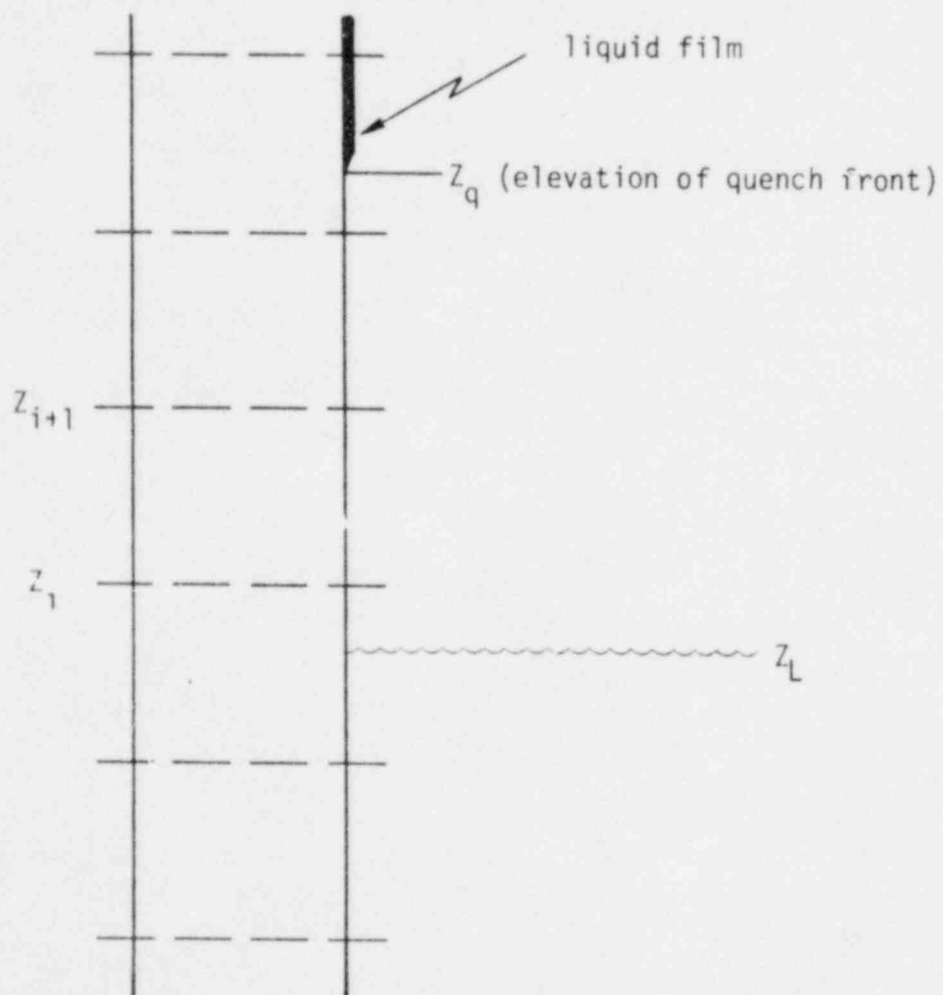


Figure 4.2 Bypass: Heat Transfer from Channels

5.0 SUPPLEMENTARY MODELS

5.1 PHASE SEPARATION MODELS

FLEX allows the user four options for determining phase separation and the resultant mixture level within a system node. Option number one assumes the node to be homogeneous with the mixture level equal to the height of the node. The second option assumes complete separation of the phases, and the liquid level is given by

$$Z_L = (1.0 - \alpha) H \quad (5.1)$$

where Z_L is the liquid level, α is the node average void fraction and H is the height of the node. The third and fourth options allow the calculation of a mixture void fraction based on drift flux theory or Wilson bubble rise theory, respectively.

5.1.1 Drift Flux Phase Separation Model

The third option utilizes the drift flux model to determine the phase distribution (void fraction) beneath the two phase mixture level. The drift flux phase separation model in FLEX is based on the assumptions that the flow is gravity dominated and that the liquid fraction above the two-phase mixture level is negligibly small. The model is illustrated in Figure 5.1.

The FLEX node within which the model is applied is subdivided into N subnodes, each with its cross sectional area A_i and height H_i , all of which are input by the user. The A_i and H_i may differ from subnode to subnode. The flow solution (see Section 2) specifies the inlet mass flow rate and density to the node from which the inlet superficial velocity is obtained

$$j_{g,in} = \frac{W_{g,in}}{\rho_g A_{in}} \quad (5.2)$$

The system solution also provides the rate of change of pressure, $\frac{dP}{dt}$, the fill energy transport rate, q_{fill} (Eq. 2.6), and the heat transfer rate into each subnode, $q_{c,i}$. (see Appendix A).

The rate of generation of vapor due to depressurization is given by

$$W_{fg}(p) = \frac{dP}{dt} [M_f(\frac{\partial h}{\partial P}^f - v_f) + M_g(\frac{\partial h}{\partial P}^g - v_g)] h_{fg}^{-1} \quad (5.3)$$

It is assumed that this vapor appears uniformly within the liquid phase, and the amount of vapor generated within a given subnode, due to a change in pressure and fill injection, is consequently

$$W_{fg,i} = M_{f,i} M_{f,node}^{-1} [W_{fg}(p) + q_{fill}] h_{fg}^{-1}. \quad (5.4)$$

Providing the net vapor generation rate in the FLEX node, $W_{fg,net}$, is greater than zero, where

$$W_{fg,net} = \sum_{i=1}^N (W_{fg,i} + q_{HT,i} h_{fg}^{-1}). \quad (5.5)$$

The rate of generation of vapor within a subnode is given by

$$W_{fg,tot,i} = W_{fg,i} + q_{c,i} h_{fg}^{-1} \quad (5.6)$$

therefore,

$$j_{g,out,i} = j_{g,in,i} + W_{fg,tot,i} \rho_g^{-1} A_i^{-1}. \quad (5.7)$$

Defining the average subnode superficial vapor velocity as

$$\bar{j}_{g,i} = \frac{1}{2} (j_{g,in,i} + j_{g,out,i}) \quad (5.8)$$

The subnode average void fraction is given by the Zuber-Findlay expression⁽¹⁸⁾

$$\alpha_i = \frac{\bar{j}_{g,i}}{C_0 \bar{j}_i + U_{gj}}. \quad (5.9)$$

where C_0 is the void distribution parameter and U_{gj} is the vapor drift velocity. The drift flux relations used are:

$$C_0 = C_0(\alpha, P) \quad (5.10)$$

$$U_{gj} = U_{gj}(\alpha, P) \quad (5.11)$$

where the functional relations of Equations 5.10 and 5.11 are based on the model of Ohkawa⁽²⁸⁾.

The void fraction model assumes that the superficial liquid velocity is negligible compared to the superficial vapor velocity, or that

$$\bar{J}_i = \bar{J}_{g,i} \quad (5.12)$$

which is an excellent approximation for pool situations.

Equation 5.9 is applied successively to each subnode, beginning with the bottom subnode, until the subnode containing the two-phase mixture level is reached. The two-phase level in this subnode is defined by

$$H_{2\theta,i} = \frac{M_{f,i}}{\rho_f A_i (1-\alpha_i)} \quad (5.13)$$

where $M_{f,i}$ is the liquid mass contained in the subnode.

The subnode liquid masses are related to the total liquid mass in the node by the relation

$$M_{f,node} = \sum_{i=1}^N M_{f,i} \quad (5.14)$$

5.1.2 Wilson Bubble Rise Model

The Wilson Bubble Rise Model⁽²⁹⁾ is an approved phase separation model in ENC's Evaluation Model version of RELAP4⁽³⁰⁾. In addition, the experimental swell test data from which the Wilson model was developed was representative of JP-BWR lower plenum LOCA conditions. Thus, the Wilson Bubble Rise Model was included as an option for a phase separation model.

5.2 UPPER PLENUM MODEL

The presence of ECC sprays in the upper plenum results in the occurrence of phenomena such as droplet entrainment and countercurrent flow which do not exist in other FLEX system nodes. A special model is therefore provided to describe fluid behavior in the upper plenum.

The FLEX upper plenum model is shown schematically in Figure 5.2. The ECC spray flow W_{spray} is input by the user as a function of time or pressure. The values for the inlet boundary flows W_{CCFL} and W_{in} are computed by the FLEX core model and supplied as boundary conditions to the system model. The mixture level, H_{20} , is computed using the drift flux phase separation model discussed in Section 5.1. The nodal flow, W_{out} , results from the general system flow solution discussed in Section 2. The droplet entrainment flow $W_{\text{ent,d}}$ and the surface liquid entrainment flow, $W_{\text{ent,l}}$, result from interaction

between the upward flowing steam and the ECC spray droplets and from entrainment of droplets by steam flow through a liquid pool, respectively. If the upper plenum mixture level is below the elevation of the spray sparger the spray droplet entrainment mechanism is activated. Steam flow at a pool surface is the assumed mechanism if the mixture level exceeds the sparger elevation (Z'_{spray}).

5.2.1 Spray Droplet Entrainment

The model for spray droplet entrainment assumes a characteristic droplet size corresponding to a critical Weber Number of $12^{(9)}$ as given by:

$$d_m = \frac{12\sigma}{\rho g U_n^2} \quad (5.15)$$

where σ is the surface tension and U_n is the liquid velocity in the spray nozzles. The droplet sizes are further assumed to follow the Nukiyama-Tanasawa distribution as given by:⁽⁹⁾

$$N(d) = \frac{32d^2}{d_m^3} e^{-4\frac{d}{d_m}} \quad (5.16)$$

which has a most likely or mean droplet size of $d = d_m/2$.

The critical droplet size for entrainment is calculated assuming a balance between gravity and drag forces, and is described by:

$$d_e = \frac{0.75 \rho_g C_D V_g^2}{g(\rho_f - \rho_g)} \quad (5.17)$$

where V_g is the vapor velocity and the drag coefficient is consistent with Equation 3.41. The droplets which are entrained are thus those with diameters less than or equal to d_e . The volume fraction of droplets with diameters less than or equal to d_e , ϕ , can be obtained by integrating the size distribution as given by:

$$\phi = \frac{\int_0^{d_e} d^3 N(d) dd}{\int_0^{\infty} d^3 N(d) dd} \quad (5.18)$$

where $N(d)$ is given by Equation 5.16. The total droplet mass entrainment rate is then computed as:

$$W_{ent} = \phi(W_{spray}) \quad (5.19)$$

where W_{spray} is the mass flow of the spray into the upper plenum.

5.2.2 Entrainment From a Pool

If the mixture level in the upper plenum is above the spray spargers, the entrainment mechanism is different from that described above. The method applied in FLEX is an extension of the empirical method of Wilson^(20,21) which described the entrainment rate as a function of pressure and height from the mixture level to the volume outlet. A critical superficial steam velocity is defined at which the entrained moisture reaches 1%. The critical entrainment velocity is given by:

$$j_{g,e} = [2.93 - 1.1675 \times 10^{-3} (P - 15.0)] H_0^{0.42} \quad (5.20)$$

where $j_{g,e}$ is the critical velocity in ft/sec, P is pressure in psia, and H_0 is the height from mixture level to the upper plenum outlet in feet. For H_0 less than one, H_0 is assumed equal to one. Equation (5.20) is a curve fit to an expression presented by Wilson⁽²¹⁾, and is valid for pressures from 15 to 1000 psia (0.1 to 6.9 MPa). The entrainment rate is calculated by:

$$W_{ent} = j_g^2 \rho_g A \left(\frac{0.01}{j_{g,e}} \right) \left[1.0 - \left(\frac{0.01}{j_{g,e}} \right) j_g \right]^{-1} \quad (5.21)$$

In the event that j_g becomes greater than $j_{g,e}$ the liquid content of the flow at the top of the upper plenum is assumed to be that which would occur if the fluid in the upper plenum were assumed to be homogeneous.

5.3 CRITICAL FLOW MODELS

The determination of choked break mass flow rates is made using either the Moody⁽²²⁾ or Homogeneous Equilibrium Model (HEM)⁽²³⁾ as specified

on the user input with the Moody model used for licensing analysis. The critical mass flux is given by Moody as:

$$G = \text{MAX} \left[K \left\{ \frac{2gJ (h_o - h_f - xh_{fg})}{K(1-x) v_f + xv_g]^2 [(K^2-1)x + 1]} \right\} \right]^{1/2} \quad (5.22)$$

where the maximum occurs at a slip ratio of $K = (v_g/v_f)^{1/3}$. Choking with the HEM model occurs when the fluid velocity reaches the homogeneous equilibrium sound speed. The HEM critical mass flux is given by;

$$G = \frac{2gJ [h_o - h_f - xh_{fg}]^{1/2}}{(1-x) v_f + xv_g} \quad (5.23)$$

The above equations are implemented in FLEX in tabular form using tables generated as a function of pressure and quality. The user must also specify a discharge coefficient C_B such that the break mass flow rate becomes

$$W = C_B G_{\text{choke}} A \quad (5.24)$$

As noted in Section 2, the pressure and fluid quality at the break is used to enter the choking tables. A break mass flow rate is also computed assuming unchoked flow at the break. The break mass flow rate used is the minimum of the choked and unchoked values, and is used as a boundary condition in the system flow solution (Section 2) and in the determination of the depressurization rate as described below.

5.4 SYSTEM DEPRESSURIZATION RATE

During a LOCA the reactor system depressurization is determined by the flow of mass and energy across the system boundaries and the flashing and expansion of the fluid within the system. The system depressurization

rate is computed and the pressure at a reference point in the system is then given by:

$$P_{\text{ref}} = P_0 + \frac{dP}{dt} \Delta t. \quad (5.25)$$

The depressurization rate $\frac{dP}{dt}$ is computed using the relation developed below.

Considering the BWR system as a single large volume containing saturated liquid, saturated vapor and superheated vapor (in the core only) as illustrated in Figure 5.3, one can write the total internal energy as

$$\bar{U} = M_f u_f + M_g u_g + M_v u_v \quad (5.26)$$

and taking the derivative with respect to time

$$\dot{\bar{U}} = \frac{d\bar{U}}{dt} = \dot{M}_f u_f + \dot{M}_g u_g + \dot{M}_v u_v + M_f \frac{du_f}{dt} + M_g \frac{du_g}{dt} + M_v \frac{du_v}{dt}. \quad (5.27)$$

The First Law gives for the entire system

$$\dot{\bar{U}} = Q_s + Q_v - \Sigma W_f h_f - \Sigma W_g h_g. \quad (5.28)$$

The total volume of the system is

$$V = M_f v_f + M_g v_g + M_v v_v \quad (5.29)$$

and since the volume is constant,

$$\dot{V} = 0 = \dot{M}_f v_f + \dot{M}_g v_g + \dot{M}_v v_v + M_f \dot{v}_f + M_g \dot{v}_g + M_v \dot{v}_v. \quad (5.30)$$

The mass derivatives are

$$\dot{M}_f = -\Sigma W_f - W_{fg} \quad (5.31)$$

$$\dot{M}_g = -\Sigma W_g + W_{fg} - W_{gv} \quad (5.32)$$

$$\dot{M}_v = W_{gv}. \quad (5.33)$$

Combining the preceding equations and making use of the fact that along the saturation line

$$\frac{d}{dt} = \frac{dP}{dt} \frac{\partial}{\partial P}$$

one obtains the relation

$$\begin{aligned} & \frac{u_{fg}}{v_{fg}} (\Sigma W_f v_f + \Sigma W_g v_g) - Q_s - Q_v + P(v_f W_f + v_g W_g) + W_{gv} (u_v - u_g) + M_v \frac{du_v}{dt} \\ & = \frac{dP}{dt} \left[M_f \left(-\frac{\partial u_f}{\partial P} + \frac{u_{fg}}{v_{fg}} \frac{\partial v_f}{\partial P} \right) + M_g \left(-\frac{\partial u_g}{\partial P} + \frac{u_{fg}}{v_{fg}} \frac{\partial v_g}{\partial P} \right) + M_v \frac{u_{fg}}{v_{fg}} \frac{\partial v_g}{\partial P} \right]. \end{aligned} \quad (5.34)$$

In deriving Equation 5.34 it was assumed that the density of superheated vapor is the same as saturated vapor; this assumption is justified since the mass of superheated vapor is small relative to the total system mass.

The superheated vapor is assumed to exist only in the active core region, and is produced only by heat transfer to vapor (Q_v). Writing the continuity and First Law relations for the superheated region alone, one obtains, after rearranging

$$Q_v = W_{gv} (u_v - u_g) + M_v \frac{du_v}{dt} + M_v P \frac{dP}{dt} \frac{\partial v_g}{\partial P}. \quad (5.35)$$

Substituting (5.35) into (5.34) and solving for $\frac{dP}{dt}$ yields

$$\frac{dP}{dt} = \frac{Q_s \left(\frac{v_{fg}}{h_{fg}} \right) - \Sigma W_f v_f - \Sigma W_g v_g}{M_f \left[\frac{v_{fg}}{h_{fg}} \left(\frac{\partial h_f}{\partial P} - v_f \right) - \frac{\partial v_f}{\partial P} \right] + M_g \left[\frac{v_{fg}}{h_{fg}} \left(\frac{\partial h_g}{\partial P} - v_g \right) - \frac{\partial v_g}{\partial P} \right] - M_v \frac{\partial v_g}{\partial P}} \quad (5.36)$$

which is used by FLEX to determine the rate of pressure change of the system at any point in time. It is assumed that $\frac{dP}{dt}$ is the same in every FLEX node, including the core and bypass regions.

The Q_s term appearing in Equation 5.36 is the net heat transfer rate into the saturated liquid phase only, and is assumed to produce saturated vapor.

5.5 PASSIVE HEAT CONDUCTORS IN SYSTEM VOLUMES

The slab heat conduction model used in FLEX is a one-dimensional finite element solution of the heat conduction equation based on the Method of Weighted Residuals (MWR) and employs the Galerkin Approach⁽²⁶⁾. The model has five degrees of freedom and can treat two different materials. Within each of the two regions, a quadratic temperature profile is used.

The general one-dimensional heat conduction equation solved by this method is

$$\frac{d}{dx} \left(k \frac{dT}{dx} \right) + \rho''' = \rho c \frac{dT}{dt} \quad (5.37)$$

which is subject to arbitrary initial conditions and convective boundary conditions. See Appendix A for a detailed discussion of this passive heat conductor model.

5.6 EQUATION OF STATE

The equation of state used in the core and system models was obtained from the HAMBO⁽²⁴⁾ computer code. The coolant saturation properties are represented by a polynomial curve fit of the Keenan and Keyes⁽²⁵⁾ steam tables and have errors of less than 1% in the pressure range of 14.7 - 2400 psia (0.1 to 16.4 MPa). The curve fit is of the form:

$$f(x) = C_1 + C_2x + C_3x^2 + C_4x^3 + C_5x^5 + \dots \quad (5.38)$$

where $f(x)$ is the required saturation property. X is $\ln P$ at low pressures and $(\ln P)^{-7}$ at high pressures (generally greater than 450 psia or 3.1 MPa).

5.7 COUPLING OF THE CORE AND SYSTEM MODELS

As indicated previously, the core and system models are coupled through boundary conditions at interfaces located at the inlet and exit of the core region. As discussed in this section, the term core model includes both the core and bypass regions.

Figure 5.4 illustrates this coupling. The system model provides the inlet flow to the core as a boundary condition. The maximum allowable liquid flow into the core from the upper plenum is discussed in Section 5.8. The core model is called once at the beginning of each time step, and calculates the remaining inlet and outlet flows, in addition to the pressure drop across the core and bypass region and the other variables shown on the right hand side of Figure 5.4. The system model then solves for the system flows assuming the core conditions to be known. The lower plenum pressure and the vapor flow rate into the core become the boundary conditions supplied to the core for the next time step.

5.8 SPRAY LIQUID AVAILABILITY MODEL

When the spray systems are spraying ECC liquid into the upper plenum and there is no two-phase pool above the core, the availability of spray liquid to the active core and bypass regions is apportioned according to the areas above the respective regions.

The total cross-sectional area of the upper plenum is

$$A_{up} = \frac{\pi}{4} D_{up}^2 \quad (5.39)$$

where D_{up} is the diameter of the upper plenum. The area above the fuel bundles is

$$A_{core} = N_{asm} (L_{chan}^2) \quad (5.40)$$

where N_{asm} is the total number of fuel assemblies and L_{chan} is the inside dimension of the fuel channels.

The mass flow rate of spray liquid available to the active core region is

$$W_{core,max} = (W_{spray} - W_{ent}) A_{core} A_{up}^{-1} \quad (5.41)$$

The mass flow rate of spray liquid available to the bypass region is

$$W_{bypass,max} = (W_{spray} - W_{ent})(1 - A_{core} A_{up}^{-1}). \quad (5.42)$$

W_{spray} is the spray mass flow rate, including the liquid produced by condensation in the upper plenum, and W_{ent} is the rate of entrainment of spray liquid out of the upper plenum and into the downcomer region (see Section 5.2). Equations 5.41 and 5.42 specify the maximum allowable flow rates of liquid into the core region; the minimum of the CCFL flow (Equation 3.31) and the maximum allowed liquid downflow (Equation 5.41 or 5.42) is used.

For the case where a two-phase mixture level exists in the upper plenum, the maximum allowed liquid flow rate from the upper plenum is based on the criterion that no more liquid can be taken out of the upper plenum than is already there. As for the case discussed previously with no liquid pool, the smaller of the mass depletion and CCFL flows is used.

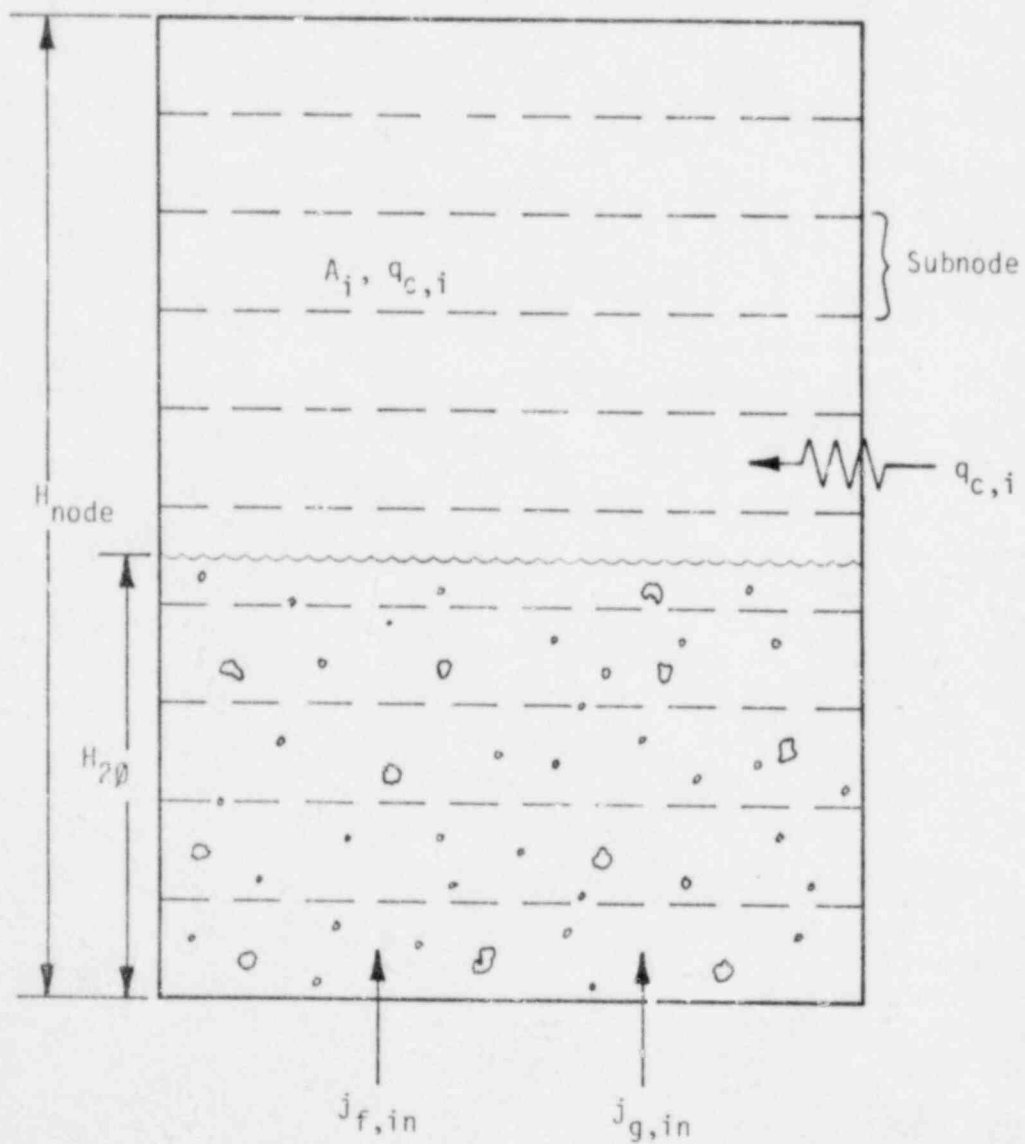


Figure 5.1 FLEX Drift Flux Phase Separation Model

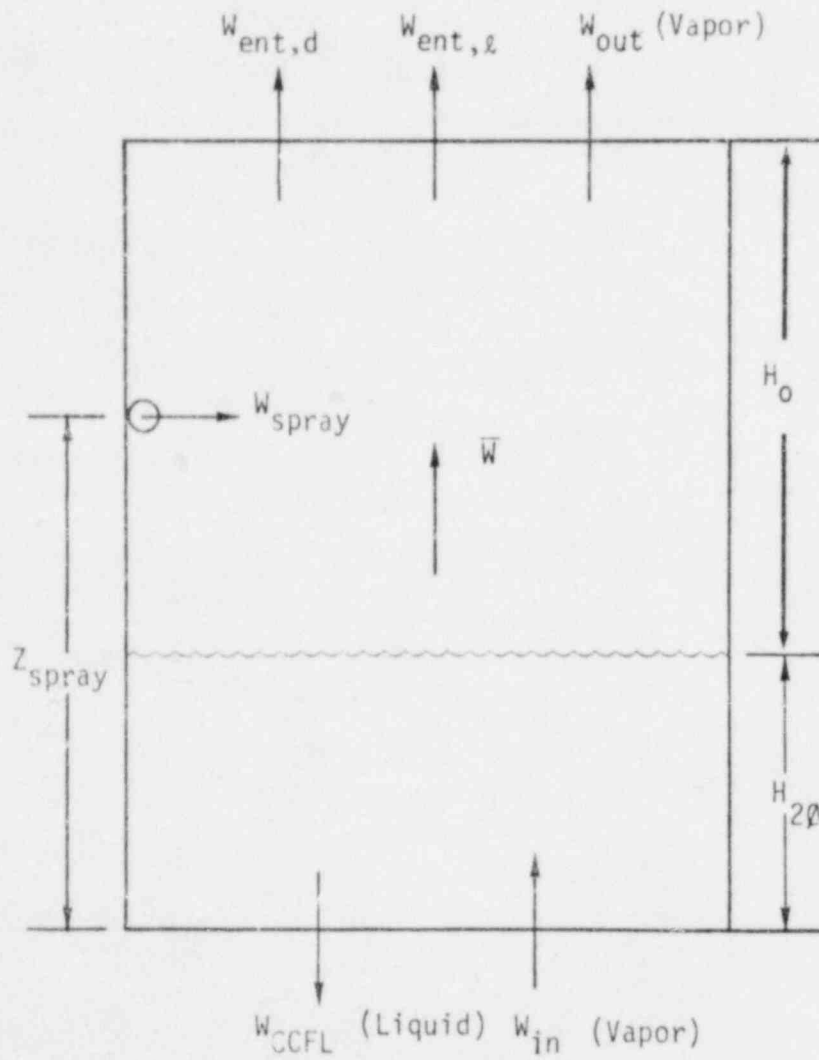
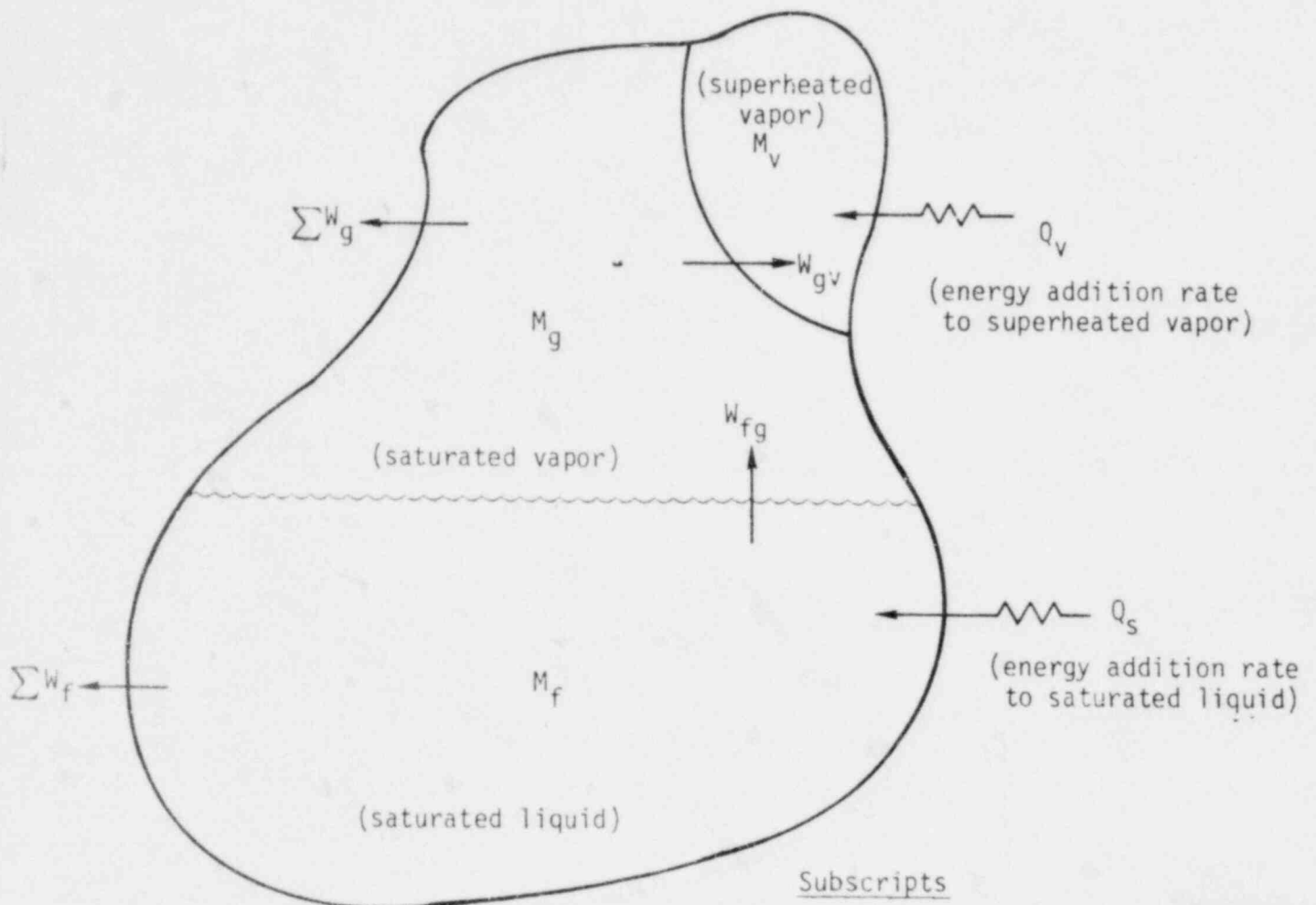


Figure 5.2 FLEX Upper Plenum Schematic

Subscripts

f = saturated liquid
 g = saturated vapor
 v = superheated vapor

Figure 5.3 - Illustration of Depressurization Model

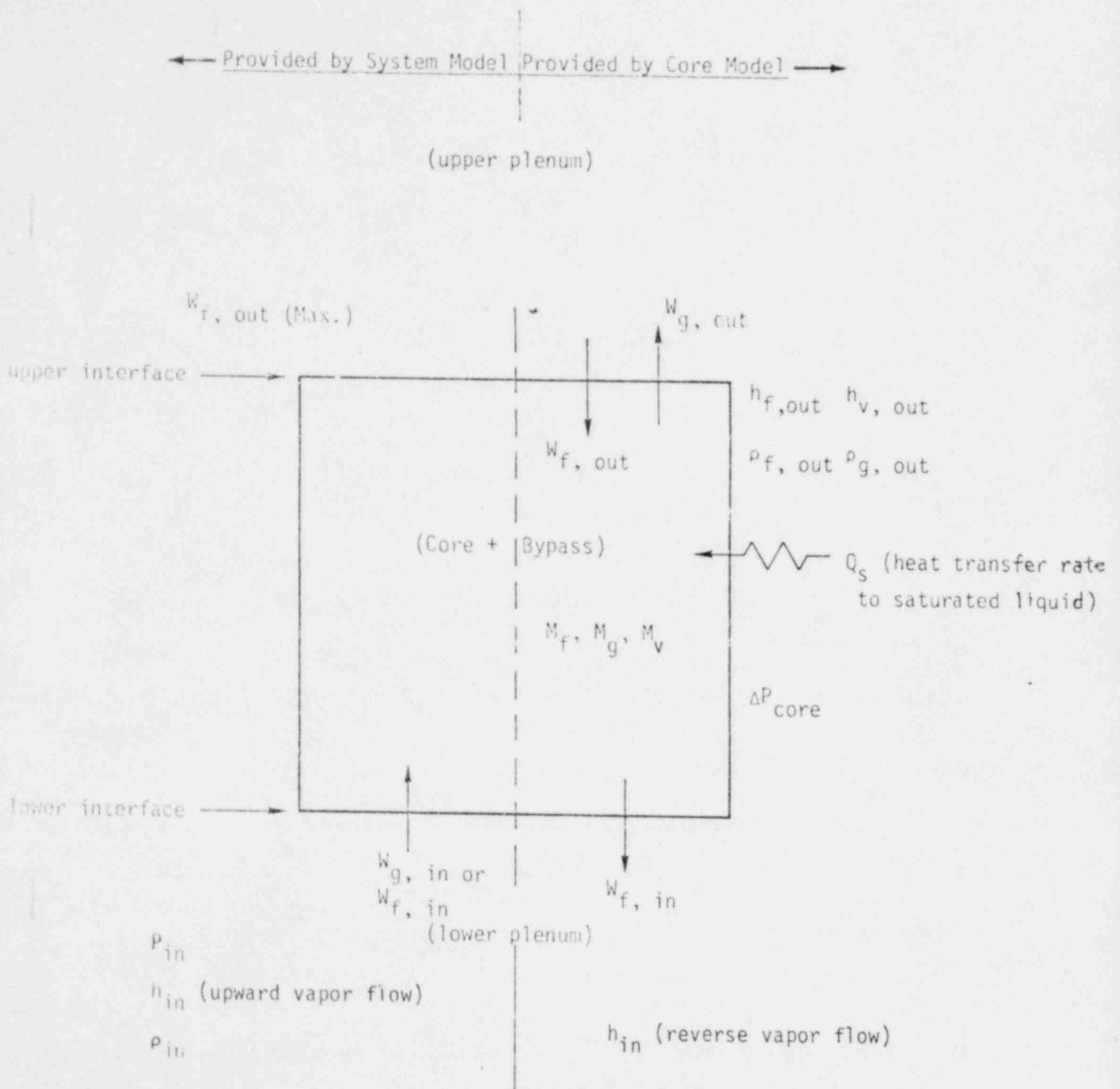


Figure 5.4 - Coupling of Core and System Models

6.0 REFERENCES

- 1) Appendix K to 10 CFR 50.
- 2) Idaho National Engineering Laboratory, "RELAP4/MOD5, A Computer Program for Transient Thermal-Hydraulic Analysis of Nuclear Reactors and Related Systems," ANCR-NUREG-1335, September 1976.
- 3) Jensen, S. E. and Jensen, R. T., "Exxon Nuclear Company WREM-Based Generic PWR ECCS Evaluation Model Update ENC WREM-IIA," XN-NF-78-30, August 1978.
- 4) Jeppson, R. W., "Analysis of Flow in Pipe Networks," Ann Arbor Science, Ann Arbor, Michigan, 1976.
- 5) Bird, R. B., et al., "Transport Phenomena," John Wiley and Sons, New York, 1960.
- 6) Baroczy, C. J., "A Systematic Correlation for Two-Phase Pressure Drop," NAA-SR-MEMO-11858, March 11, 1966.
- 7) Carnahan, B., Luther, H. A., and Wilkes, J. O., "Applied Numerical Methods," John Wiley and Sons, New York 1969.
- 8) Holman, J. P., Heat Transfer, McGraw-Hill, 1976.
- 9) Wallis, Graham B., "One-Dimension Two-Phase Flow," McGraw-Hill, 1969.
- 10) Yuen, M. C. and Chen, L. W., "Heat Transfer Measurements of Evaporating Liquid Droplets," Int. J. Heat Mass Transfer, Vol. 21, pp. 537-542, 1978.
- 11) NEDO-20566-1, "Analytical Model for LOCA in Accordance with 10 CFR 50 Appendix K - Amendment N-1 Calculation of Low Flow Film Boiling Heat Transfer for BWR LOCA Analyses," January 1977.
- 12) Siegel, Robert and Howell, John, R., "Thermal Radiation Heat Transfer," McGraw-Hill, 1972.
- 13) Anderson, J.G.M., and Hensen, P., "Two-Dimensional Heat Conduction in Rewetting Phenomena," Report No. NGRHAV-D-6, Danish AEC Research Establishment Riso, Denmark, June 1974.
- 14) Sun, K. H., and Fernandez, "Countercurrent Flow Limitation Correlation for BWR Bundles During LOCA, ANS Transaction, Vol. 27, pp. 605-606, 1977.

- 15) Pushkina, O.L., and Sorokin, Y.L., "Breakdown of Liquid Film Motion in Vertical Tubes", Heat Transfer-Soviet Research, pp. 1,5,56 1969 .
- 16) "Analytical Model for Bottom Reflooding Heat Transfer in Light Water Reactors (The UCFLOOD Code)", EPRI NP-756, August 1978.
- 17) John, James E.A., and Haberman, William L., "Introduction to Fluid Mechanics", Prentice-Hall Inc., 1971.
- 18) Collier, J.G., "Convective Boiling and Condensation", McGraw-Hill Book Company, New York 1972 .
- 19) "General Electric Company Analytical Model for Loss-of-Coolant Analysis in Accordance with 10 CFR 50 Appendix K", NEDO-20566, January 1976.
- 20) Wilson, J.F. and Grenda, R.J., "Removal of Entrained Moisture from Steam Using Natural Separation and Mechanical Dryers", ACNP-6105, April 15, 1961.
- 21) Wilson, J.F., et al., "Primary Separation of Steam from Water By Natural Separation", Joint US/Euratom R & D Program AT911-1, 1186, Allis Chalmers, April 15, 1965.
- 22) Moody, F.J., "Maximum Flow Rate of a Single Component, Two-Phase Mixture", Journal of Heat Transfer - Transactions of ASME, 87, N.1, February 1965, pp. 134-142.
- 23) Starkman, E.S., et al., "Expansion of a Very Low Quality Two-Phase Fluid Through a Convergent-Divergent Nozzle", Journal of Basic Engineering - Transactions of ASME, 86, No.2, June 1964, pp. 247-256.
- 24) Bowring, R.W., "HAMBO - A Computer Program for the Subchannel Analysis of the Hydraulic and Burnout Characteristics of Rod Clusters, Part 2 : The Equations", AEEW - R582, (1968).
- 25) Keenan, J.H. and Keyes, F.G., "Thermodynamic Properties of Steam", John Wiley and Sons, New York (1958).
- 26) Finlayson, B.A., "The Method of Weighted Residuals and Variational Principles", Academic Press, 1972.
- 27) Huebner, K.H., "The Finite Element Method for Engineers", John Wiley and Sons, 1975.
- 28) Ohkawa, K. and Lahey, R. T., Jr., "The Analysis of Proposed BWR Inlet Flow Blockage Experiments in PBF", Rensselaer Polytechnic Institute, Department of Nuclear Engineering, Troy, New York, December 1978.

- 29) NEDO-10329, "Loss-of-Coolant Accident and Emergency Core Cooling Models for G.E. Boiling Water Reactors, April 1971.
- 30) "Safety Evaluation by USNRC on RELAP4-EM/ENC28B," (ENC Letter dated October 30, 1978), Forwarded by NRC Letter from T. A. Ippolito to W. S. Nechodom dated March 30, 1979.

7.0 NOMENCLATURE

Except where specifically indicated otherwise in the text, the nomenclature used in this report is as follows:

A	m^2	Cross-sectional area
a	nd	Absorptance
B	W/m^2	Radiosity
Bi	nd	Biot Number
C	nd	Loss coefficient
C_p	$J/(kg \cdot ^\circ C)$	Specific heat
C_o	nd	Drift flux distribution parameter
d	m	Diameter
D	m	Hydraulic diameter
E	W/m^2	Black body thermal emission
f	nd	Fanning friction factor
F	N/m^3	Force; Radiation Angle Factor
g	M/s^2	Gravitational acceleration
G	m	Mass flux
h	$W/(m^2 \cdot ^\circ C)$	Convective heat transfer coefficient
h	J/kg	Enthalpy
H	m	Height
j	m/s	Volumetric flux (superficial velocity)
J	nd	Junction

NOMENCLATURE (Continued)

k	W/(m . °C)	Thermal conductivity
K	nd	Loss coefficient, Kutateladze No., slip ratio
L	m	Length, loop equation
M	Kg	Mass
N, n	nd	Number
Nu	nd	Nusselt Number
P	N/m ²	Pressure (static)
Pe	nd	Peclet number
Pr	nd	Prandtl number
p	W	Power
p'	W/m	Power per unit length
p'''	W/m ³	Power per unit volume
q	W	Heat transfer rate
q'	W/m	Heat transfer rate per unit length
q''	W/m ²	Heat transfer rate per unit area
q'''	W/m ³	Heat transfer rate per unit volume
Q	W	Heat transfer rate
R	nd	Ratio, relative
Re	nd	Reynolds number
S	Kg/(s . m ³)	A source of mass
t	s	Time
T	°C	Temperature
u	m/s	Velocity
\bar{u}	J/Kg	Specific internal energy

NOMENCLATURE (Continued)

U	m/s	Velocity
U_{gj}	m/s	Drift flux velocity
\bar{U}	J	Total internal energy
V	m^3	Volume
w	kg/(s . m)	Flow rate per unit of perimeter
W	kg/s	Mass flow rate
We	nd	Webber number
X	nd	Channel outside dimension
x	nd	Quality, vertical height of fall film front
y	m	Distance from bottom of core to mixture level
z	m	Vertical coordinate
Z	m	Vertical height
<u>Greek</u>		
α	nd	Volume fraction (of vapor if not subscripted)
γ	nd	Mixture level void fraction
δ	m	Thickness
ϵ	nd	Emittance
ν	m^3, μ	Specific volume
ρ	kg/m^3	Density
σ	N/m	Surface tension
τ	nd	Transmittance
Γ	$kg/(s . m^3)$	Mass interchange between phases
θ	nd	Dimensionless temperature
ϕ	nd	Droplet fraction
ψ	nd	Mass entrainment fraction

NOMENCLATURE (Continued)Subscripts

A	Acceleration
b	Bypass
B	Break, Region B of Bypass
c	Channel, Conductor
d	Droplet
D	Droplet, Drag
e	Entrainment
ex	Extra
f	Film, Saturated liquid
fg	Change of phase
F	Friction
g	Saturated vapor
G	Body forces
h	Enthalpy transport
i	Inlet, dummy index
j	Dummy index
l	Liquid, Lower bypass junction
l	Liquid
L	Level
m	Mixture, Mean
n	Nozzle
o	Outlet, Original

NOMENCLATURE (Continued)

q	Quench
r	Rod, relative
s	Saturated
T	Total, Region T of bypass
u	Upper bypass junction
v	Vapor
w	Wall

Superscripts

.	Time derivative
~	Formation value
*	Formation value
-	Average value

APPENDIX A

PASSIVE HEAT CONDUCTOR MODEL

The slab heat conduction model used in FLEX is a one-dimensional finite element solution of the heat conduction equation based on the Method of Weighted Residuals (MWR) and employs the Galerkin Approach⁽²⁶⁾. The model has five degrees of freedom and can treat two different materials. Within each of the two regions, a quadratic temperature profile is used.

The general one-dimensional heat conduction equation solved is

$$\frac{d}{dx} \left(k \frac{dT}{dx} \right) + p''' = \rho c \frac{dT}{dt} \quad (\text{A.1})$$

which is subject to the following boundary conditions:

$$T(t=0, x) = f(x) \quad (\text{A.2})$$

$$-k \frac{dT}{dx}(x=0, t) = h(x=0, t) (T_{\infty}(x=0, t) - T(x=0, t))$$

$$k \frac{dT}{dx}(x=L, t) = h(x=L, t) (T_{\infty}(x=L, t) - T(x=L, t)).$$

In the MWR, the equation residual is defined as

$$R = \frac{d}{dx} \left(k \frac{dT}{dx} \right) + p''' - \rho c \frac{dT}{dt}. \quad (\text{A.3})$$

This residual is forced to vanish in an average sense over the domain of interest as

$$\int_0^L W_j R dx = 0 \quad (\text{A.4})$$

where $j = 1, 2, \dots, n$ undetermined parameters and W_j is some weighting coefficient.

In FLEX, Equation A.4 is expanded to include two distinct regions as

$$\int_0^{L_1} W_j R dx + \int_{L_1}^L W_j R dx = 0. \quad (\text{A.5})$$

In region one (from 0 to L_1) the temperature profile is chosen as

$$T(x) = N_1 T_1 + N_2 T_2 + N_3 T_3 \quad (\text{A.6})$$

where T_1 is at $x=0$, T_2 at $x=\frac{L_1}{2}$ and T_3 is at $x=L_1$.

The quadratic influence coefficients are⁽²⁷⁾

$$N_1 = 2\left(\frac{x}{L_1}\right)^2 - 3\left(\frac{x}{L_1}\right) + 1 \quad (\text{A.7})$$

$$N_2 = -4\left(\frac{x}{L_1}\right)^2 + 4\left(\frac{x}{L_1}\right)$$

$$N_3 = 2\left(\frac{x}{L_1}\right)^2 - \left(\frac{x}{L_1}\right).$$

In region two (from L_1 to L) the temperature profile is chosen as

$$T(x) = N_3+ T_3 + N_4 T_4 + N_5 T_5$$

where T_4 is at $x = \frac{L-L_1}{2} + L_1$ and T_5 is at $x=L$. The quadratic influence coefficients are

$$N_{3+} = 2\left(\frac{x-L_1}{L-L_1}\right)^2 - 3\left(\frac{x-L_1}{L-L_1}\right) + 1 \quad (\text{A.8})$$

$$N_4 = -4\left(\frac{x-L_1}{L-L_1}\right)^2 + 4\left(\frac{x-L_1}{L-L_1}\right)$$

$$N_5 = 2\left(\frac{x-L_1}{L-L_1}\right)^2 - \left(\frac{x-L_1}{L-L_1}\right)$$

Using the Galerkin approach, the weighting coefficients (W_j) are chosen as the quadratic influence coefficients. That is

$$\begin{aligned}
 W_i &= N_i \quad 0 \leq x \leq L_1 & i &= 1, 2 \\
 &= 0 \quad L_1 < x \leq L \\
 W_3 &= N_{3-} \quad 0 \leq x \leq L_1 \\
 &= N_{3+} \quad L_1 \leq x \leq L \\
 W_i &= 0 \quad 0 \leq x \leq L_1 & i &= 4, 5 \\
 &= N_i \quad L_1 \leq x \leq L
 \end{aligned} \tag{A.9}$$

etc. Carrying out the operations indicated in Equation A.5 produces the following five equations which are written in matrix form as:

$$\begin{aligned}
 &\begin{bmatrix} 7KL_1+h_1+4RC_1 & -8KL_1+2RC_1 & KL_1-RC_1 & 0 & 0 \\ & 16KL_1+16RC_1 & -8KL_1+2RC_1 & 0 & 0 \\ & & 7KL_1+4RC_1+7KL_2+4RC_2 & -8KL_2+2RC_2 & KL_2-RC_2 \\ & & & 16KL_2+16RC_2 & -8KL_2+2RC_2 \\ & & & & 7KL_2+h_5+4RC_2 \end{bmatrix} \begin{bmatrix} T_1 \\ T_2 \\ T_3 \\ T_4 \\ T_5 \end{bmatrix}^{n+1} = \\
 &\quad \text{(Symmetric)} \\
 &\begin{bmatrix} 4RC_1 & 2RC_1 & -RC_1 & 0 & 0 \\ & 16RC_1 & 2RC_1 & 0 & 0 \\ & & 4RC_1+4RC_2 & 2RC_2 & -RC_2 \\ & & & 16RC_2 & 2RC_2 \\ & & & & 4RC_2 \end{bmatrix} \begin{bmatrix} T_1 \\ T_2 \\ T_3 \\ T_4 \\ T_5 \end{bmatrix}^n + \begin{bmatrix} h_1 T_{\infty 1} \\ 0 \\ 0 \\ 0 \\ h_5 T_{\infty 5} \end{bmatrix}^{n+1} + \begin{bmatrix} PL_1 \\ 4PL_1 \\ PL_1+PL_2 \\ 4PL_2 \\ PL_2 \end{bmatrix}^{n+1} \tag{A.10} \\
 &\quad \text{(Symmetric)}
 \end{aligned}$$

where

$$\begin{aligned}
 KL_1 &= \frac{k_1}{3L_1} & KL_2 &= \frac{k_2}{3(L-L_1)} \\
 RC_1 &= \frac{(\rho C)_1 L_1}{30 \Delta t} & RC_2 &= \frac{(\rho C)_2 (L-L_1)}{30 \Delta t} \\
 PL_1 &= \frac{P_1^- L_1}{6} & PL_2 &= \frac{P_2^- (L-L_2)}{6}
 \end{aligned} \tag{A.11}$$

In the above, the subscript 1 denotes values in the region from 0 to L_1 and the subscript 2 denotes values in the region from L_1 to L . In Equation A.10, h_1 and $T_{\infty 1}$ are the environmental values for the $x=0$ side of the slab and h_5 , $T_{\infty 5}$ for the $x=L$ side of the slab. The superscript n is a counter on time. The form given in Equation A.10 is stable and will not oscillate due to truncation error. For the case where only one material is used, L_1 may be chosen to be anyplace between 0 and L . At present, for such cases, L_1 is chosen as $L/10$ and the $x=0$ side is always chosen to be the side with the greatest Biot number. An insulated boundary condition can be obtained by setting h_5 to zero.

In order to obtain axial resolution of the heat transfer from a heat slab in a FLEX node that contains a mixture level, the user may specify that the slab be subdivided into axial subnodes. The heat transfer coefficient is varied to account for the mixture level by using $h=h_\ell$ below the two-phase level, $h=h_v$ above the two-phase level, and linearly weighting the coefficients by the mixture level in the subnode containing the mixture level,

$$h = \frac{(Z-Z_b)}{\Delta Z} h_\ell + \frac{(Z_t-Z)}{\Delta Z} h_v \quad (\text{A.12})$$

where

ΔZ = subnode height

Z = mixture level

Z_b = elevation of bottom of subnode

Z_t = elevation of top of subnode

h_ℓ = heat transfer coefficient below level

h_v = heat transfer coefficient above level

APPENDIX BVERIFICATION OF FLEX WITH FCTF DATA
SAMPLE COMPARISONSTABLE OF CONTENTS

<u>Section</u>	<u>Page</u>
B.0 INTRODUCTION AND SUMMARY	B-1
B.1 FCTF DESCRIPTION	B-2
B.2 SPRAY TEST WITH STEAM UPDRAFT	B-3
B.3 REFLOOD TEST	B-4

LIST OF FIGURES

<u>Figure</u>		<u>Page</u>
B-1	FUEL COOLING TEST FACILITY SCHEMATIC	B-7
B-2	FCTF FUEL ASSEMBLY AND INTERNALS	B-8
B-3	COMPARISON OF MIDPLANE CLAD TEMPERATURES FROM TIME OF SPRAY INITIATION	B-9
B-4	AVERAGE TEMPERATURE TRANSIENT - ACTUAL	B-10
B-5	AVERAGE TEMPERATURE TRANSIENT - PREDICTED BY FLEX	B-11
B-6	COMPARISON OF VAPOR GENERATION RATES FROM TIME OF SPRAY INITIATION	B-12
B-7	COMPARISON OF LIQUID PENETRATION RATES FROM TIME OF SPRAY INITIATION	B-13
B-8	PREDICTED VS. ACTUAL ASSEMBLY PRESSURE DROP FROM TIME OF REFLOOD	B-14
B-9	LIQUID FLOW INTO MIDPLANE NODE FROM TIME OF REFLOOD	B-15

LIST OF TABLES

<u>Table</u>		<u>Page</u>
B-1	FCTF TEST CONDITIONS	B-6

APPENDIX B
VERIFICATION TO FCTF DATA
SAMPLE COMPARISONS

B.0 INTRODUCTION AND SUMMARY

This Appendix presents sample comparisons between FLEX code predictions and ECCS spray and reflood data from ENC's Fuel Cooling Test Facility (FCTF).

ENC has significantly upgraded the FCTF so ECCS spray and reflood tests can be performed that are representative of JP-BWR conditions. Steam updraft and reflood capability have been expanded and a simulated jet pump has been added. The testing program is designed to develop a thermal hydraulic data base for FLEX qualification and is representative of average core conditions. An initial spectrum of tests (shakedown) have been run in the modified facility to confirm the capability to test under JP-BWR conditions.

In order to make these comparisons, the FLEX core model was extracted from a preliminary version of the FLEX code and run on a standalone basis. The geometry and material properties of the FCTF bypass region and electrically heated bundle were incorporated into FLEX. The submodels of FLEX were used as developed from general literature theory and data; no tuning of submodels was performed.

The test runs selected for comparison were part of the shakedown test runs and included a spray and a reflood test. Since these tests were part of a shakedown program data uncertainties were not established.

Section B.1 briefly discusses the FCTF facility, Section B.2 discusses the spray test comparisons and Section B.3 presents the reflood test comparisons.

Considering the preliminary nature of the model and data, the agreement between the FLEX predictions and data is remarkable. Thus these comparisons show that FLEX will be capable of analyzing the thermal hydraulics of the JP-BWR refill and reflood period.

B.1 FCTF DESCRIPTION

The Fuel Cooling Test Facility (FCTF) has been used to conduct NJP-BWR ECCS tests, and is now located at ENC's Horn Rapids site. The FCTF capabilities have been upgraded to better simulate jet pump BWR ECCS conditions. Steam updraft and reflood capability has been increased and a simulated jet pump has been added. Schematics of the FCTF test loop and fuel assembly are shown in Figures B-1 and B-2 respectively.

The facility is capable of delivering sprays to the upper plenum and bypass. The reflood portion of a reactor transient can also be simulated via flood lines in the lower plenum. Steam lines are available for steam injection into the lower plenum and bypass in order to simulate vaporization in the reactor lower plenum.

The test facility contains a full-scale electrically heated mock-up of an ENC JP-BWR 8x8 fuel assembly and channel. Core inlet orificing is simulated. The simulated fuel bundle consists of one unpowered rod, (the inert rod), and 63 electrically heated rods which are constructed so as to produce a chopped cosine axial power distribution. The rods

are instrumented with thermocouples at each foot of elevation, with the exception of the 11 ft and 9 ft. levels. Spacer grids and an upper tie plate are included in the simulated assembly. Thermal shields, designed to approximate the hydraulic and geometric boundary conditions around each channel in the reactor, surround the channel.

FCTF instrumentation provides for measurement of the following parameters: selected pressure drops; bundle power; rod, channel, and thermal shield temperatures; various flow temperatures, and steam and liquid flow rates sufficient to determine a mass balance.

B.2 SPRAY TEST WITH STEAM UPDRAFT

The initial conditions and boundary flows for Test 2901, a spray test with steam updraft, are listed in Table B-1. For FLEX simulations, the test bundle was divided into five nodes of equal length with one rod type (average rod). Comparisons of predicted and experimental values are shown in Figures B-3 through B-7.

Figure B-3 shows the average rod temperature comparison. The value plotted from FLEX is the midplane nodal temperature for the average heated rod while the data is the average of all thermocouples at the six foot elevation. These temperatures agree quite well. Figures B-4 and B-5 show the temperature profile at 100 second intervals for the average rod. The measured results of Figure B-4 show the average of all thermocouple readings at eleven elevations, while Figure B-5 shows the five nodal temperatures calculated by the FLEX core model. These plots also compare favorably.

Figure B-6 presents the calculated and experimental test assembly vapor generation rates, including the bypass region. The injected updraft steam has not been included in either curve. After an initial transient, the predicted and actual values compare well. The initial difference is related to the amount of vapor generation predicted from the FCTF bypass which includes non prototypic thermal shields and/or experimental uncertainties early in the test.

Figure B-7 is a comparison of the liquid penetration rates. These values are again the combined totals for the assembly and the bypass. A negative value on the liquid penetration indicates flow in the downward direction. Initially, due to the higher calculated vapor generation, the predicted penetration is less than observed. The quasi-steady state penetration prediction late in the transient is also somewhat less than the measured value. In the first two minutes the differences between the predictions and data could be caused by the averaging that is inherent in the use of collection tanks.

The overall conclusion from the spray test comparison is that FLEX slightly underpredicts the bundle temperatures, overpredicts the vapor generation rate and underpredicts the liquid penetration. This indicates that FLEX core model in its present form contributes conservatively (later than actual) to the time of reflood prediction.

B.3 REFLOOD TEST

Test 3806 was a reflood with spray test. The parameters of importance are listed in Table B-1. This test was modeled beginning from the time

of reflood. Figures B-8 through B-9 present the FLEX results vs. the data for this test.

Figure B-8 compares the total bundle pressure drops. The pressure drop is a measure of the mixture level and entrainment. Thus the good agreement between the pressure drop predictions and data support the mixture level and entrainment models in FLEX.

Figure B-9 shows the predicted liquid flow rate into the midplane node. The sharp rise in liquid flow rate at 14 seconds is taken as the time the two phase fluid reaches the midplane (time of hot node reflood) and the Appendix K reflood coefficient of $25 \text{ BTU/hr.ft}^2.\text{F}^\circ$ ($0.142 \text{ Kw/m}^2.\text{C}^\circ$) is to be applied. The change from Appendix K spray to reflood coefficients is sufficient to cause the slope of peak clad temperature to change from a positive to a negative value (PCT turnover). 14 seconds is also the time FLEX predicts the turnover of the midplane rod temperature. The measured average and peak rod temperatures at the midplane both turnover at 9 seconds. (Time of actual hot node reflood). Thus, this data comparison indicates that the FLEX prediction of time of hot node reflood is conservative relative to data by about 5 seconds.

Table B-1

FCTF Test Conditions

	<u>Test</u> <u>2901</u>	<u>Test</u> <u>3806</u>
Type of test	Spray	Reflood
Initial power, KW	216	240
Fuel Assembly Spray, gpm	4.6	4.6
Channel Spray, gpm	1.4	-
Reflood Flow, in/sec.	-	3.1
Injected Lower Plenum Steam, lb _m /hr	200	-
Injected Bypass Steam, lb _m /hr	50	-

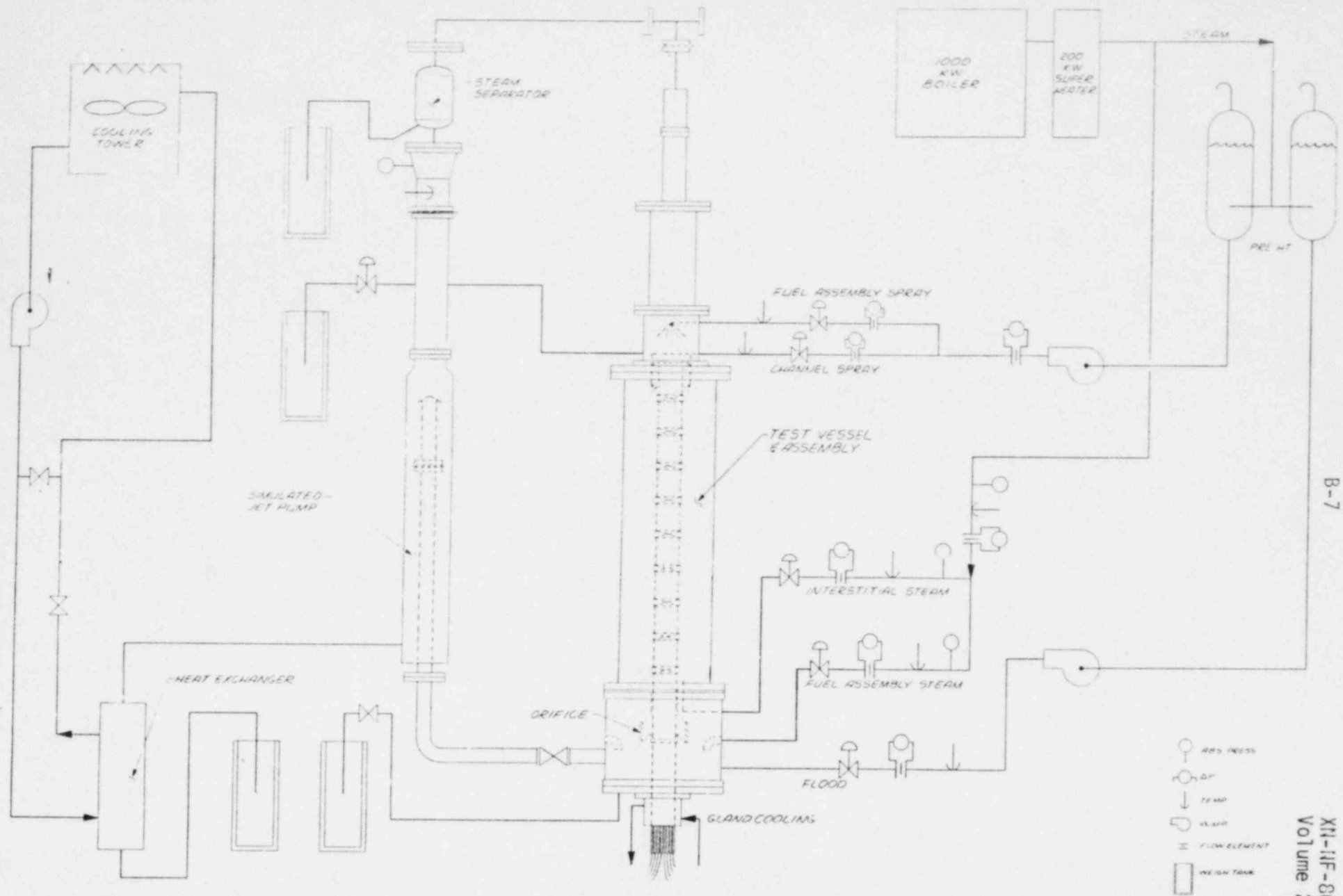


Figure B-1 Fuel Cooling Test Facility Schematic

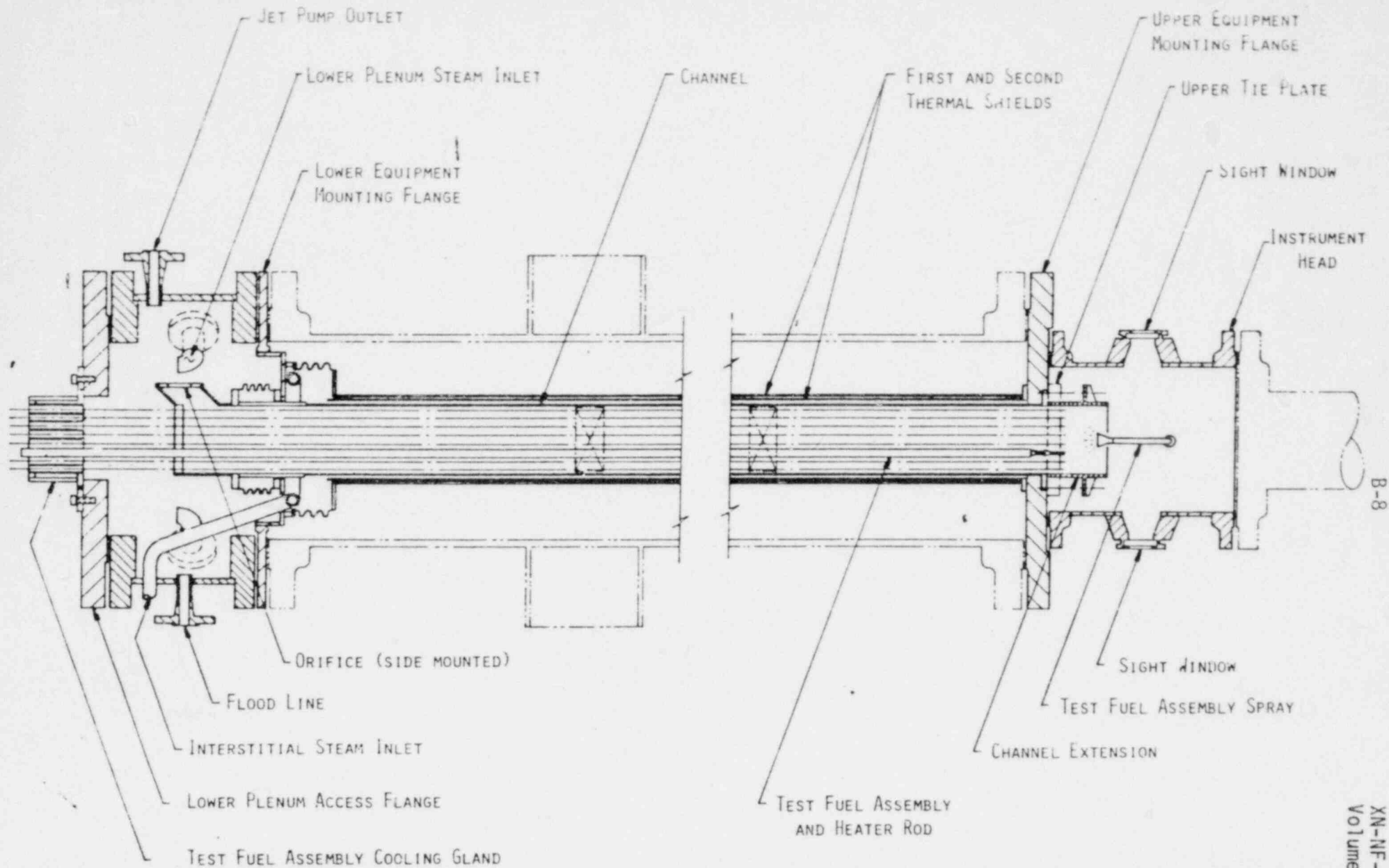
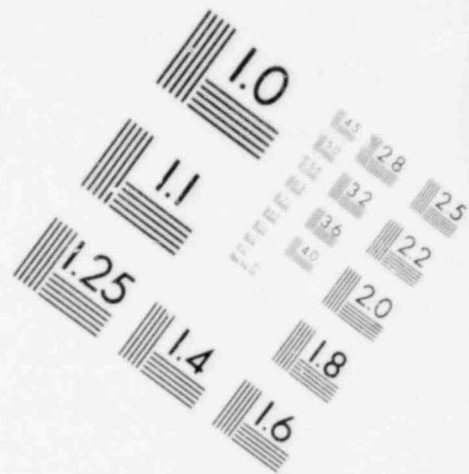
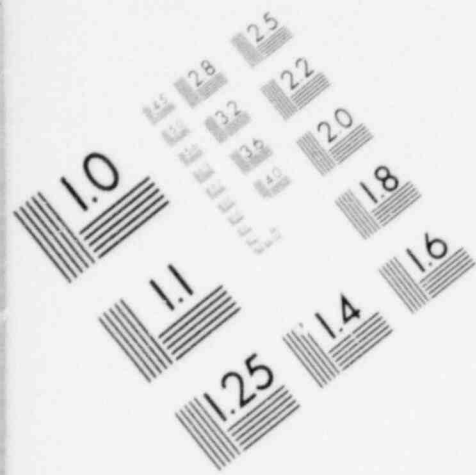


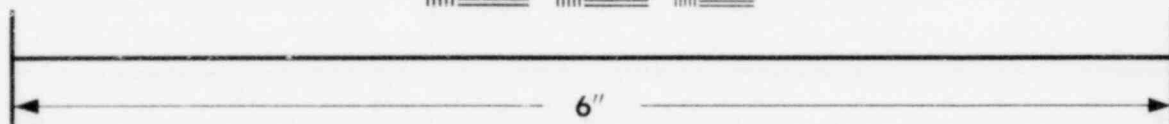
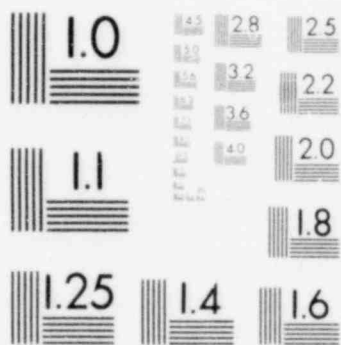
Figure B-2 FCTF Fuel Assembly and Internals

Figure B-3 Comparison of Midplane Clad Temperatures from Time of Spray Initiation

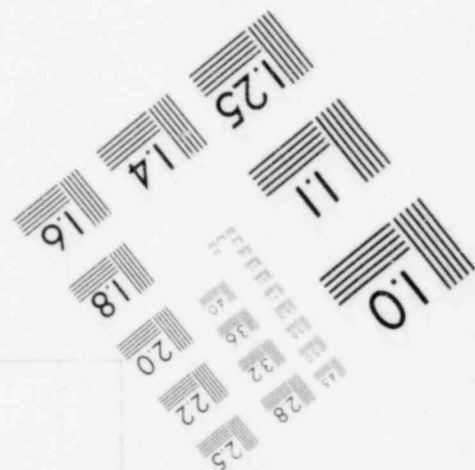
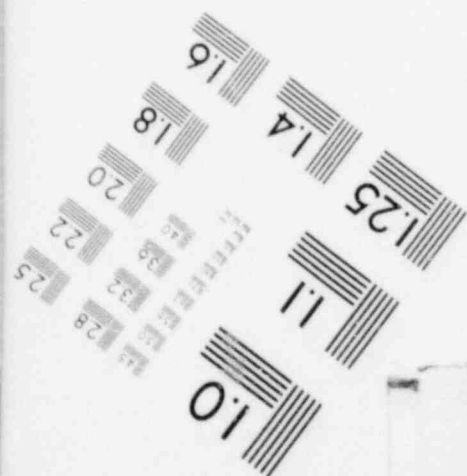
Figure B-4 Average Temperature Transient - Actual



**IMAGE EVALUATION
TEST TARGET (MT-3)**



MICROCOPY RESOLUTION TEST CHART



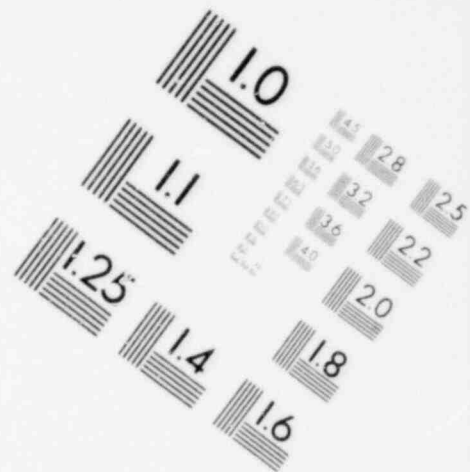
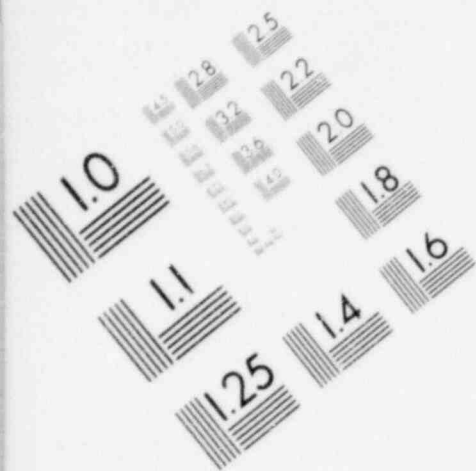
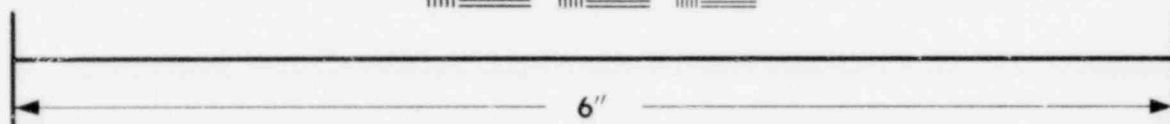
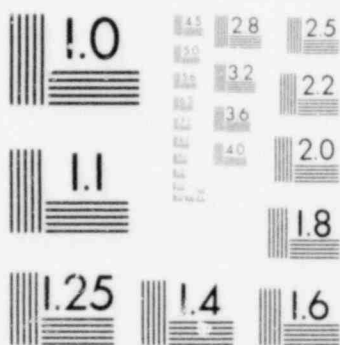


**IMAGE EVALUATION
TEST TARGET (MT-3)**



MICROCOPY RESOLUTION TEST CHART

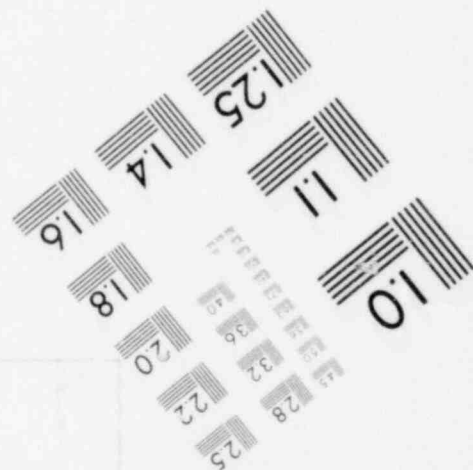
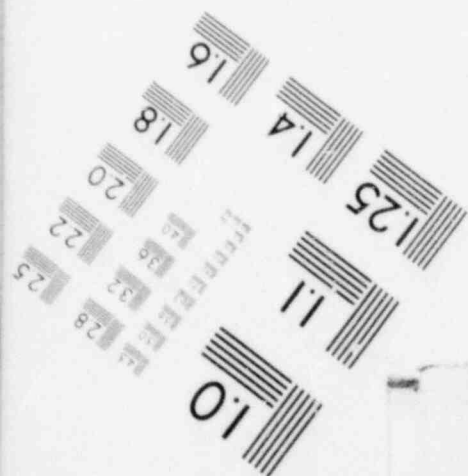


Figure B-5 Average Temperature Transient - Predicted by FLEX

Figure B-6 Comparison of Vapor Generation Rates from Time of Spray Initiation

B-13

XII-NF-80-19(NP)
Volume 2B

Figure B-7 Comparison of Liquid Penetration Rates from Time of Spray Initiation

Figure B-8 Predicted vs. Actual Assembly Pressure Drop from Time of Reflood

Figure B-9 Liquid Flow into Midplane Node from Time of Reflood

XN-NF-80-19(NP)

Volume 2B

07/31/80

FLEX:

A COMPUTER CODE FOR JET PUMP BWR REFILL AND REFLOOD ANALYSIS

Distribution

RE Collingham

GF Owsley

USNRC/GF Owsley (20)

Document Control (5)